AD NUMBER

AD865731

LIMITATION CHANGES

TO:

Approved for public release; distribution is unlimited.

FROM:

Distribution authorized to U.S. Gov't. agencies only; Test and Evaluation; JAN 1970. Other requests shall be referred to Air Force Flight Dynamics Laboratory, ATTN: FDFE, Wright-Patterson AFB, OH 45433.

AUTHORITY

AFFDL ltr dtd 25 Jun 1971

AFFDL-TR-69-54

THE PREDICTION OF INTERNAL VIBRATION LEVELS OF FLIGHT VEHICLE EQUIPMENTS USING STATISTICAL ENERGY METHODS

ROBERT W. SEVY

DAVID A. EARLS

TECHNICAL REPORT AFFDL-TR-69-54

JANUARY 1970

AIR FORCE FLIGHT DYNAMICS LABORATORY
AIR FORCE SYSTEMS COMMAND
WRIGHT-PATTERSON AIR FORCE BASE, OHIO

NOTICE

When Government drawings, specifications, or other data are used for any purpose other than in connection with a definitely related Government procurement operation, the United States Government thereby incurs no responsibility nor any obligation whatsoever; and the fact that the government may have formulated, furnished, or in any way supplied the said drawings, specifications, or other data, is not to be regarded by implication or otherwise as in any manner licensing the holder or any other person or corporation, or conveying any rights or permission to manufacture, use, or sell any patented invention that may in any way be related thereto.

This document is subject to special export controls and each transmittal to foreign governments or foreign nationals may be made only with prior approval of the Air Force Flight Dynamics Laboratory (FDFE), Wright-Patterson Air Force Base, Ohio 45433.

The distribution of this report is limited because it protects the technical know-how relating to tests and evaluation of military operational weapon systems.

Copies of this report should not be returned unless return is required by security considerations, contractual obligations, or notice on a specific document.

200 - February 1970 - CO455 - 107-2395

FOREWORD

This report covers in-house research conducted by the Air Force Flight Dynamics Laboratory, Vehicle Equipment Division, Environmental Control Branch. This study effort is in support of Project No. 1309, "Environmental Interactions," Task No. 130904, "Vibration Technology," and was conducted under the direction of Robert W. Sevy and David A. Earls. Experimental assistance was provided by Messrs. E. Ruddell and F. Stahl; data analysis and reduction by Messrs. E. Schell and H. Kinum. This report represents the work done during the period June 1965 through March 1968.

This technical report has been reviewed and is approved.

WILLIAM C. SAVAGE
Chief, Environmental Control Branch
Vehicle Equipment Division

ABSTRACT

This study is primarily concerned with the prediction of internal vibration levels in an equipment package using statistical energy methods. Modal densities, loss and coupling factors were determined theoretically and experimentally. Predicted vibration levels were derived and compared to experimental results. The energy coupling factor relating the box cover to the internal component responses was derived and compared favorably to experimental values. A generalized coupling factor is included for future applications. It is demonstrated that statistical energy methods offer a new and powerful method by which the average internal vibration levels of equipments may be predicted when the vibration field of the equipment cover is known or can be estimated.

This abstract is subject to special export controls and each transmittal to foreign governments or foreign nationals may be made only with prior approval of the Air Force Flight Dynamics Laboratory (FDFE), Wright-Patterson Air Force Base, Ohio 45433.

TABLE OF CONTENTS

TABLE OF CONTENTS (CONTD)

LIST OF ILLUSTRATIONS

LIST OF ILLUSTRATIONS (CONTD)

SYMBOLS

T_{T1} = total kinetic energy of mode set one (in-lbs)

T_{T2} = total kinetic energy of mode set two (in-lbs)

T_1 = kinetic energy per mode in box cover (in-lbs)

T_2 = kinetic energy per mode in printed circuit boards (in-lbs)

μ_1^2 = energy coupling factor (from box cover to boards)

μ = energy coupling factor (from reverberant room to box)

N_1 = total number of modes of box cover = $n_1(w)\,\Delta\omega$

N_2 = total number of modes of boards = $n_2(w)\,\Delta\omega$

η = loss factor

η_1 = true loss factor of box cover

η_{1a} = apparent loss factor of box cover

η_2 = true loss factor of boards

η_{2a} = apparent loss factor of boards

η_{21} = coupling loss factor

m_1 = mass of box cover

m_2 = mass of circuit boards

$n(f)$ = theoretical modal density (modes/CPS)

$n(f)_o$ = observed mode density

$n(f)'$ = corrected mode density

$\langle \overline{V}^2 \rangle$ = time and spatial average (mean squared velocity)

$\langle \overline{g}(\omega) \rangle$ = time and spatial average (RMS acceleration)

V = velocity (in/sec)

$S(\omega)$ = acceleration power spectral density g^2/rads per sec

a = acceleration (g's)

$\overline{p}^2$ = mean squared pressure (Newtons/meter^2)

SYMBOLS (CONTD)

ρ_a = mass density of air

c_a = velocity of sound in air (in/sec)

f = frequency (Hz)

ω = circular frequency (rads/sec)

$\Delta\omega$ = bandwidth (rads/sec)

A_p = area of box or boards (in^2)

P = perimeter of box or boards (in)

K = radius of gyration of plate (in)

c = bending wave velocity = $\sqrt{\omega K C_L}$ (in/sec)

C_L = longitudinal wave velocity (in/sec)

C'_L = corrected, or pseudo longitudinal wave velocity (in/sec)

t = plate thickness (in)

Δf = modal separation = $\frac{1}{n(f)}$ (Hz), or, desired bandwidth

Δb = modal bandwith

Q = $\frac{1}{\eta}$

f_n = modal resonance frequency (Hz)

APPENDIXES I, II, AND III

k = spring constant of stripped circuit boards (lbs/in)

k' = spring constant of fully loaded and mounted boards (lbs/in)

E = modulus of elasticity $\frac{(lbs)}{in^2}$ (stripped board)

E' = modulus of elasticity (boards loaded and mounted)

w = weight of board without components

w' = weight of board with components and stiffeners

F = static force at $\frac{\ell}{2}$ (lbs)

$\frac{\ell}{2}$ = midpoint of circuit boards (in)

SYMBOLS (CONTD)

Δ = deflection of board at midpoint (in)

b = board width (in)

SECTION I

INTRODUCTION

Intense sound and vibration fields are generated by the propulsion systems of aircraft, missiles, and by high speed flight regimes resulting in air pressure fluctuations which in turn, couple to structural surfaces. This energy couples to and through equipments to produce complex responses which may result in malfunction of internal systems and/or in fatigue failures. In order to construct an item of equipment to withstand the acoustic and vibration environment, a prediction process is required that permits the designer to estimate the response magnitudes of the internal levels over a broad frequency range.

The application of statistical energy methods to flight vehicle equipment provides a promising approach for predicting vibration levels at various regions of the equipment structure and substructure. By use of power flow analogies, the coupling behavior between the vibration source and receiver may be described and then utilized to define the time and spatially averaged vibration magnitudes which result from an external, coupled excitation representing an acoustic field or another vibration source.

This study effort consists of six sections. The first section contains a short introduction and the second section gives the approach to the study effort. The third section is a study of the modal densities of the box cover and the boards and is concerned with the development of a general equation by which the mode densities of printed circuit boards may be adjusted for mass loading effects and stiffness influences on the modal count due to the presence of mounted components and due to the addition of support stringers. The fourth section is concerned with the measurement, and derivation of the applicable loss factors that are required in order to obtain the energy coupling factor, μ_1^2. The fifth section proposes the prediction of the vibration response of the vibration response of the boards resulting from a known vibration field of the box cover. The predicted results are compared with a set of laboratory measurements. The experimental μ_1^2 is also obtained and compared to the derived form. A smoothed μ_1^2 is synthesized for tentative, future applications. Finally, the sixth section consists of conclusions and recommendations for future studies.

SECTION II
APPROACH

Consider a two element energy sharing structure which might represent, one, the outer cover of an equipment box (symbolized by subscript 1), and, two, the inner connecting elements consisting of printed circuit boards (symbolized by subscript 2).

From Reference 1 we obtain the energy relation $T_{T2} = \mu_1^2 T_{T1}$, where T_{T2} and T_{T1} are the total kinetic energies of corresponding mode sets in structures 1 and 2 and where μ_1^2 represents the energy coupling factor. The factor, μ_1^2, is equal to $\eta_{21}/(\eta_{21} + \eta_2)$ where η_{21} is the coupling loss factor arising from the mechanical joints between structures 1 and 2 and where η_2 is the true loss factor of structure 2 taken alone (removed from structure 1).

Again, in Reference 1 we note that $T_1 = \frac{m_1}{2N_1} <\overline{V}_1^2>$ and $T_2 = \frac{m_2}{2N_2} <\overline{V}_2^2>$ where $N_1 = n_1(\omega)\Delta\omega$ and $N_2 = n_2(\omega)\Delta\omega$. N_1 is the total number of modes in energy set one and N_2 is the total number of modes in energy set two and $\Delta\omega$ is the set bandwidth. T_2 and T_1 are the average, single modal energies. Substituting in $T_2 = \mu_1^2 T_1$ to solve for the mean squared velocity of the modal response, we have:

$$\frac{<\overline{V}_2^2>}{<\overline{V}_1^2>} = \frac{n_2(\omega)\, m_1}{n_1(\omega)\, m_2} \cdot \mu_1^2 \qquad (1)$$

Where $n(\omega)$ is the structural mode density, m_1 represents the structural mass and $<\overline{V}^2>$ is the space and time averaged mean square velocity. For the case of random vibration taken over a mode ensemble of bandwidth $\Delta\omega$, we set

$$\frac{<\overline{V}^2>\omega^2}{\Delta\omega} = <S(\omega)>$$

which is the spatially averaged acceleration power spectral density. Equation 1 now expresses the response of the printed circuit boards as follows:

$$<S(\omega)_2> = <S(\omega)_1> \frac{n_2(\omega)m_1}{n_1(\omega)m_2} \mu_1^2 \qquad (2)$$

where:

$$\mu_1^2 = \frac{\eta_{21}}{\eta_{21}\,\eta_2} \tag{3}$$

Similarly, by equating the power flow between an acoustic volume enclosing an equipment box one may describe the resultant vibration field of the box cover. From Reference 1 we have,

$$\frac{<\bar{a}^2>}{<\bar{p}^2>} = 2\pi^2 \frac{c_a\, n_1(\omega)}{\rho_a\, m_1} \cdot \mu \tag{4}$$

Where $<\bar{a}^2>$ is the same spatial and time averaged mean squared acceleration of the box cover resulting from a time and spatially averaged mean squared acoustic pressure $<\bar{p}^2>$. The terms c_a and ρ_a are the velocity of sound and the density of air. The term μ is more complex than μ_1^2 reflecting the coupling from box cover to board as well as the energy coupling of the reverberant room to the box. It is not intended to consider Equation 4 further in this study other than to show that by the use of energy equations, we may be able to predict vibration levels of the internal elements of an equipment package from a directly excited acoustic volume. In this study we are chiefly concerned with the prediction of the vibration level of the equipment boards when the vibration level of the box surface is known or can be estimated.

Returning to Equation 2 and the equipment box, we see that the prediction of $<S(\omega)_2>$ depends upon the determination of the modal densities of both box cover and boards, their masses, and the energy coupling factor, μ_1^2. Since structural masses are usually known, or can be estimated, it remains to determine $n_1(\omega)$, $n_2(\omega)$, and μ, if the prediction process is to be utilized. The details of this study involves the measurement and derivation of the modal densities, together with a description of a variety of loss factors whose interrelationships allow us to derive μ_1^2. These properties are then applied to an aircraft equipment which, reduced to its simplest model, is presumed to consist of an array of printed circuit boards enclosed by a sheet metal cover.

The equipment selected is an electronic equipment package and is part of the gunfire alarm and gun-fire detection system for fighter aircraft. It contains

transistorized circuitry with ten plug-in printed circuit boards stacked in two vertical columns. The box size is 15 3/8" x 9 7/8" x 7 5/8" and weighs 18 pounds. Figure 1 shows the item with the cover removed.

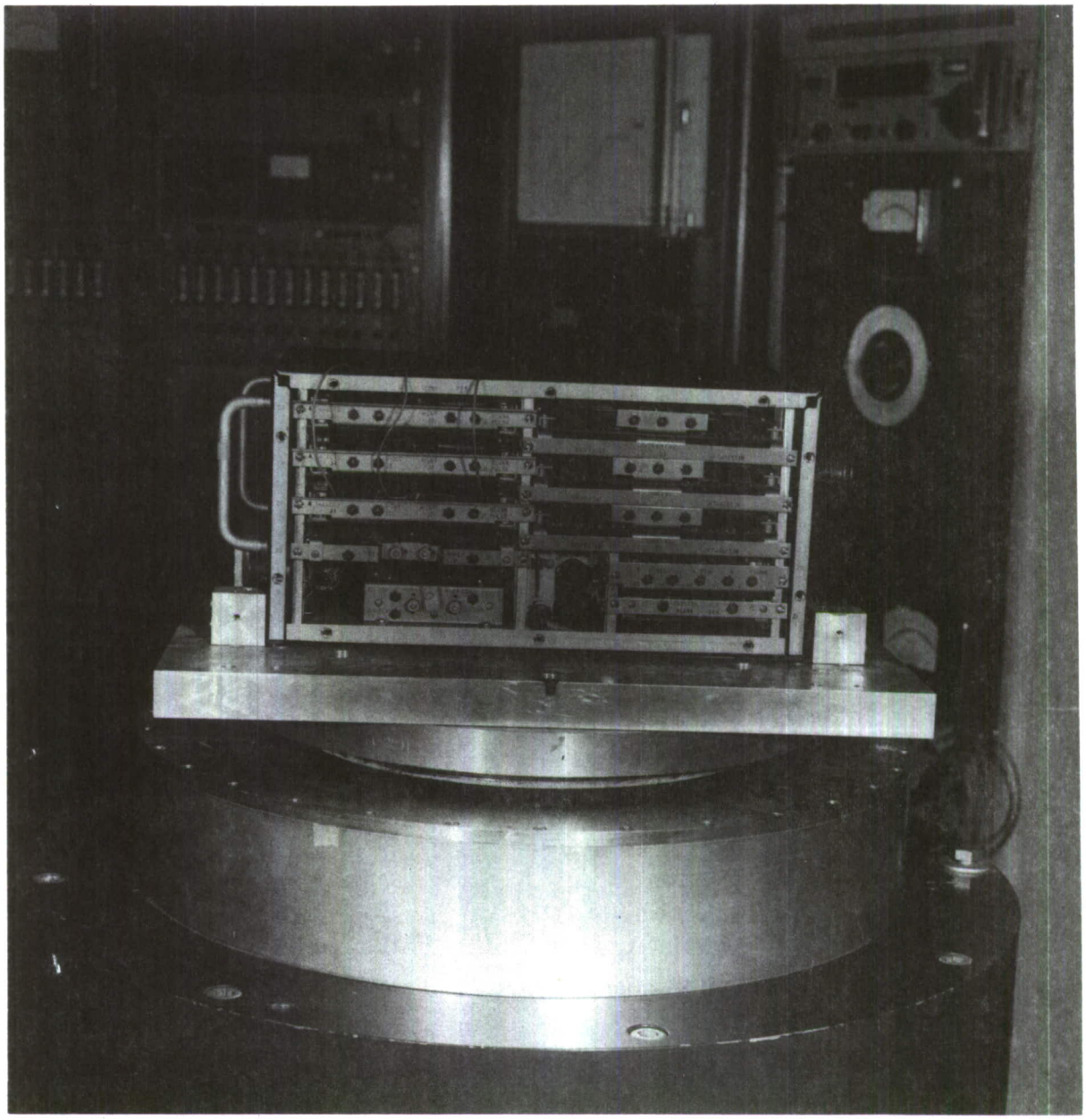

Figure 1. Equipment Box With Side Cover Removed

SECTION III
MODAL DENSITY

1. DEFINITION

The theoretical expression (Equation 3) for the modal density of a simply supported isotropic thin plate is:

$$n(\omega) \approx \frac{A_p}{4\pi KC_L} \quad \frac{P}{2\sqrt{\omega KC_L}} \tag{5}$$

where, A_p is the surface area (taken on one side), P is the surface perimeter, C_L is the longitudinal wave velocity, t is the plate thickness; and K is the radius of gyration and is equal to

$$\frac{t}{\sqrt{12}} \cdot K$$

It has been shown in past studies that the second term is negligible (over most of the frequency range) and may be dropped. Thus, the mode density becomes:

$$n(\omega) = \frac{A_p}{4\pi KC_L} \tag{6}$$

$$n(f) = \frac{A_p \sqrt{3}}{t\, C_L} \tag{7}$$

The next step is to examine the tractability of the modal density expression when applied to loaded printed circuit boards and actual box covers.

2. MODAL MEASUREMENTS OF BOARDS A AND B

Two printed circuit boards were removed from the box and measurements were made of their modal densities. One plug in board (Figure 2) approximately 8.5" x 1/16" was covered by resistors, capacitors, and transistors. The second board is approximately 8.5" x 6" x 1/16" and is heavily loaded with shift register cores along with resistor elements. For ease of identification, we shall hereafter refer to each board type as A and B respectively. Both boards are plug-ins and are secured at the end opposite the tongue with

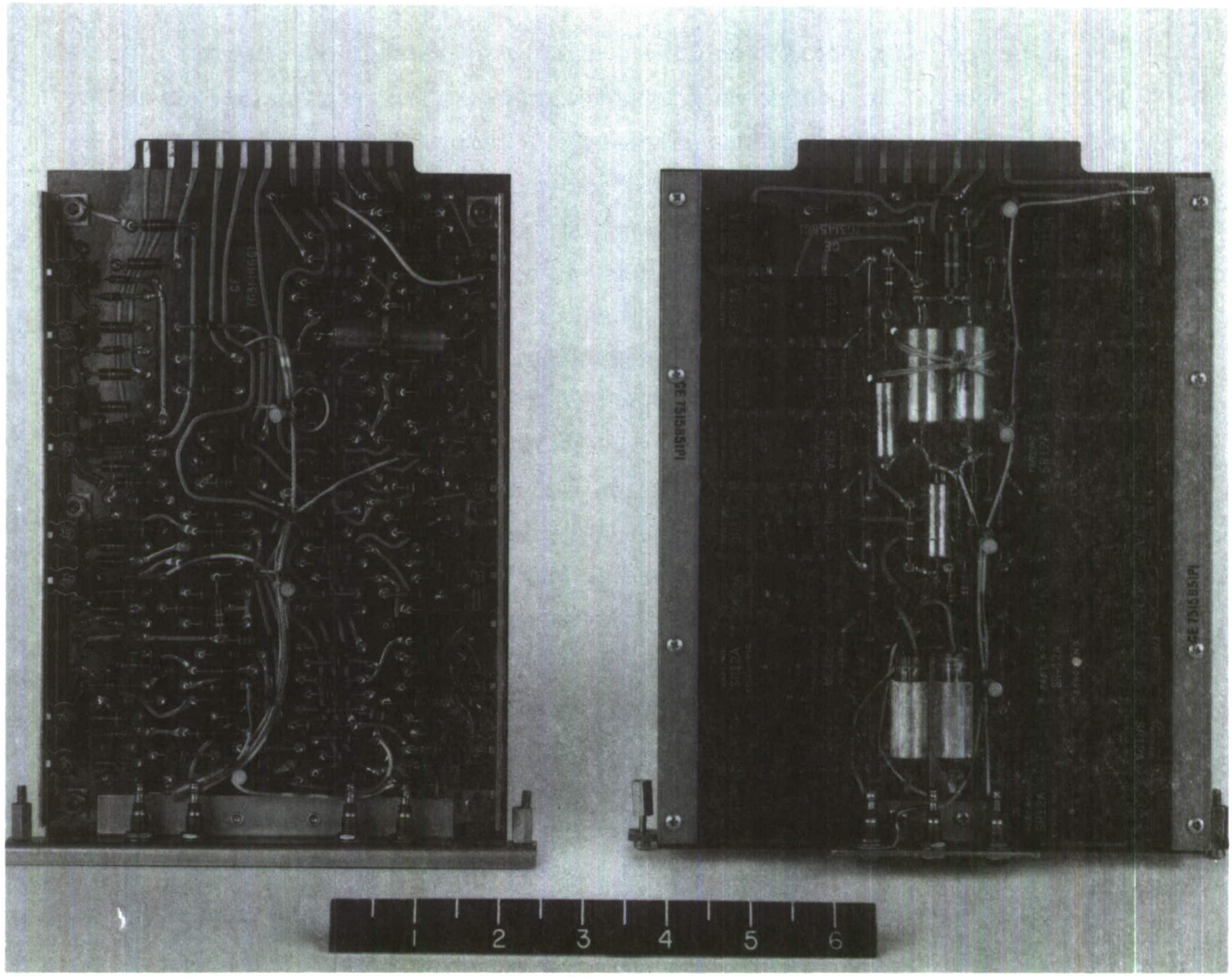

Figure 2. Plug-In Boards, Types A and B

two screws located in 5/16" square hollow aluminum rods. Boards A and B are edge bound by 1/16" aluminum angle strips that are attached to the board edges with widely spaced rivets.

A jig was constructed to hold the boards, to facilitate modal density measurements of the boards when removed from the box, and to allow close inspection of the modal patterns (Figure 3). Mounting holes were located and a mating plug-in receptacle was positioned to simulate the in situ mounting conditions with the important exception that the jig structure is sufficiently rigid as to be considered relatively lossless beyond the boundaries of the two mounting screws and the plug-in receptacle. Accelerometers (Endevco 2226) were mounted with Eastman 910 cement. Several locations per board were recorded. The amplified signal (Endevco 2614B) was coupled into a Spectral Dynamics SDS-101A analyzer using a 2 CPS crystal bandwidth chosen for good resolution of the responses. The filtered output was coupled to a Hewlett-Packard logarithmic converter (Model 60D); thence, to the Y axis of 11" x 17" Electro instruments Model 500 X-Y recorder. The X or frequency axis was supplied from a Hewlett-Packard 500c frequency converter to allow expansion of the frequency axis and thus augmenting detailed resolution of modal responses and also providing a more accurate measurement of the loss factor when using the half power method.

A Ling Electronics A-300B shaker was used. The board was subjected to 1g peak sinusoidal acceleration; slowly swept from 20 to 2000 CPS. The board was checked over the frequency range for linearity of response by increasing the input level and noting a proportionate increase in the accelerometer response.

The responses were recorded on 11" x 17" graph paper. Three records per total sweep were recorded: 25 to 100 CPS, 100 to 1000 CPS, and 1000 to 2000 CPS.

3. MODAL DENSITY OF BOARDS A AND B

The accumulative mode count for boards A and B are shown in Figures 4 and 5. A straight line was drawn through the points. The slope of the curve

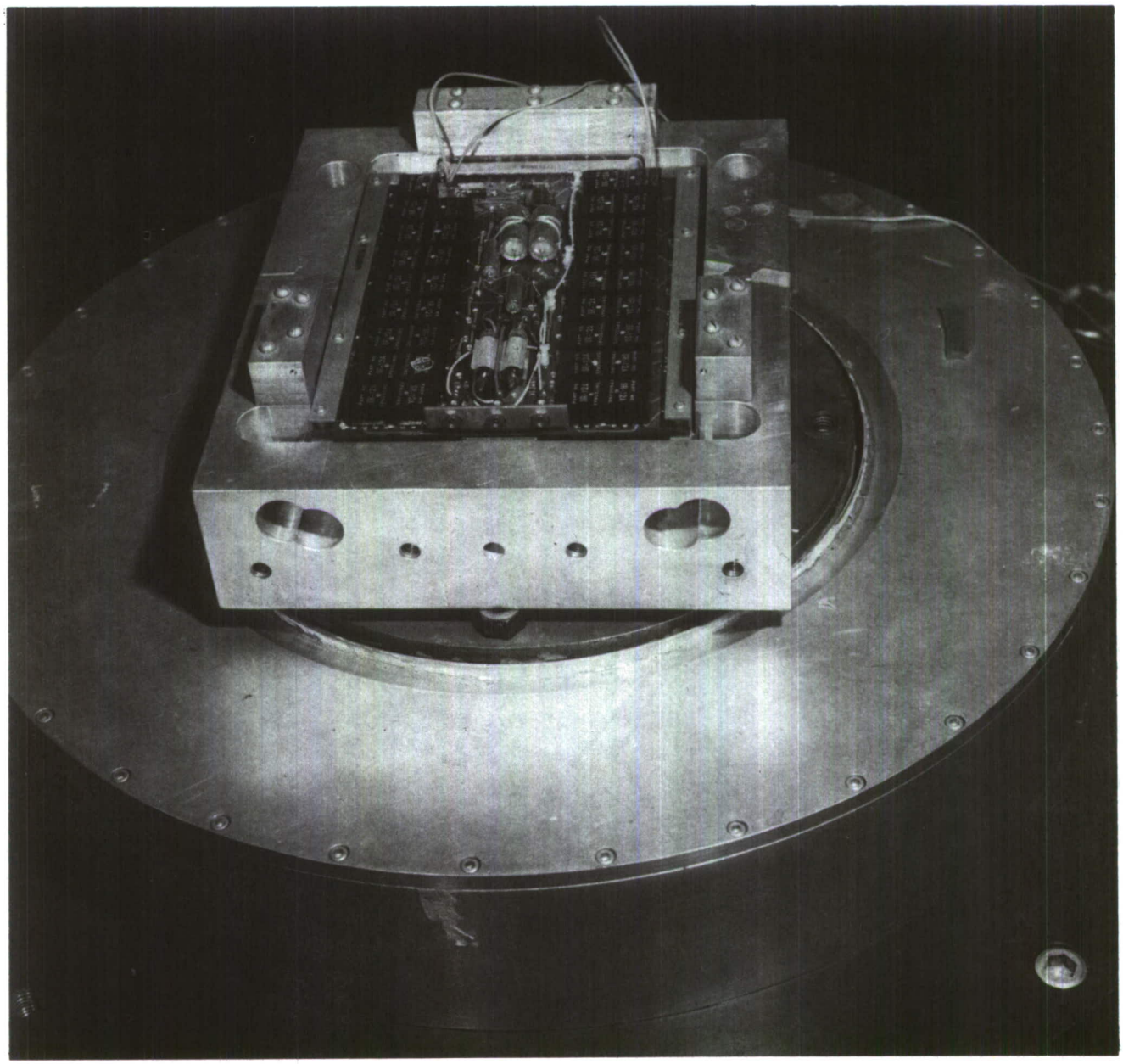

Figure 3. Test Jig Used for External Modal Measurements

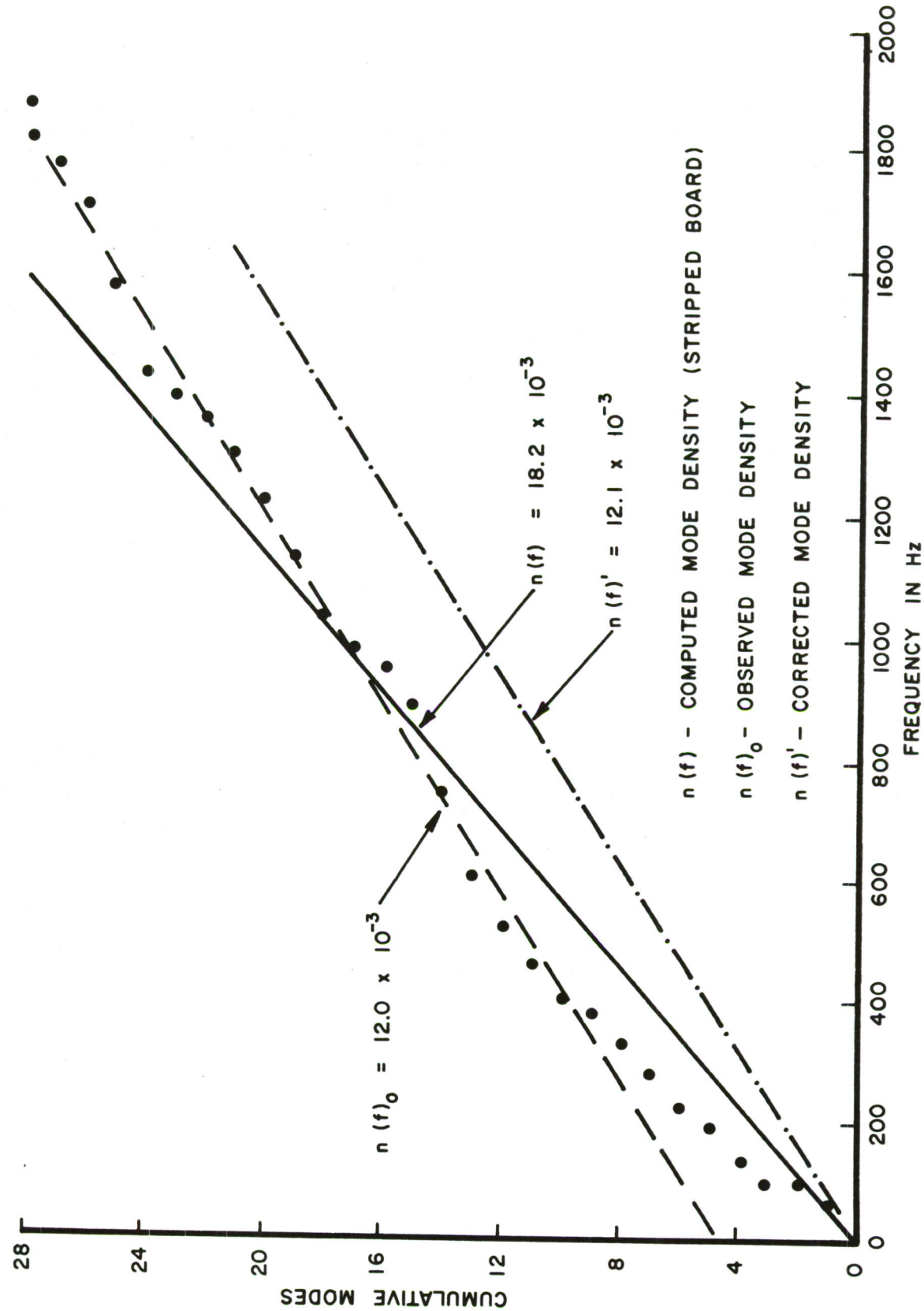

Figure 4. Cumulative Mode Count for Printed Circuit Board A, Externally Mounted

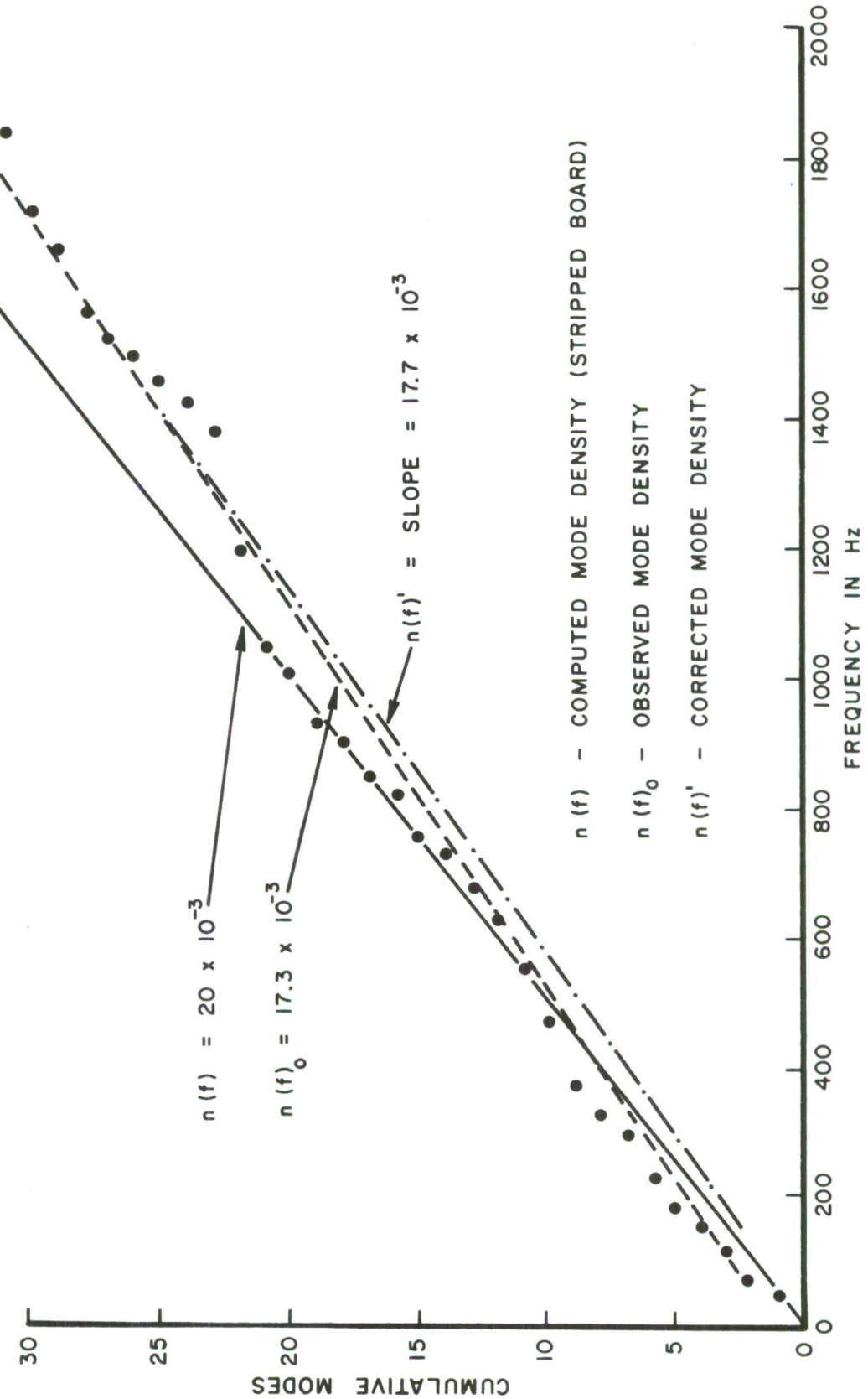

Figure 5. Cumulative Mode Count for Printed Circuit Board B, Externally Mounted

represents the observed modal density $n(f)_o$. The dashed line represents the theoretical n(f) (of the stripped boards) using Equation 7.

It is seen that the theoretical values exceed considerably the measured values-approximately 50 percent for board A and 20 percent for board B.

4. CORRECTIVE STEPS

Assuming that the difference between measured and calculated values is due primarily to the mass loading of the mounted components and the increased stiffness due to components, stiffeners, and other mounting stiffness contributions, we proceed to attempt a correction.

Recalling that,

$$n(f) = \frac{A_p \sqrt{3}}{C_L \; t}$$

Where,

$n(f)$ = mode density (modes/CPS)

A_p = the board area ($in.^2$)

t = board thickness (in.)

$C_L = \sqrt{\frac{E}{\rho}}$ the longitudinal wave velocity (in./sec)

We note that C_L describes the stiffness and mass properties. A new board is imagined having a distributed mass and stiffness equivalent to our fully loaded boards mounted in situ (the jig mounting stiffness is considered to approximate mounted conditions in the box). For the stripped boards we let:

$$n(f) = \frac{A_p \sqrt{3}}{C_L \; t}$$

and allow:

$$n(f') = \frac{A_p \sqrt{3}}{C_L' \; t}$$

The expression, $n(f)'$, represents the mode density of the fully loaded boards having an adjusted longitudinal wave velocity C_L' reflecting the stiffness and mass contributions. For the derivation of this expression see Appendixes I and II. Dividing one equation by the other and solving for $n(f)'$, we obtain,

$$n(f)' = \frac{C_L}{C_L'} \cdot n(f)$$

where C_L' is termed the adjusted, or pseudo velocity.

For board A, (computations in Appendixes I and II)
n(f) is approximately 18.2 modes/1000 CPS
and $n(f)'$ is 12.1 modes/1000 CPS

For board B, (Appendixes I and II)
n(f) is approximately 20 modes/1000 CPS
and $n(f)' = 17.7$ modes/1000 CPS

The corrected mode densities $n(f)'$ are compared to the observed values $n(f)_o$ and the computed stripped board values n(f). The plots of $n(f)'$ is also included in Figures 4 and 5.

BOARD A	BOARD B
$n(f) = 18.2$ modes/1000 CPS	$n(f) = 20.0$ modes/1000 CPS
$n(f)' = 12.1$ modes/1000 CPS	$n(f)' = 17.7$ modes/1000 CPS
$n(f)_o = 12.0$ modes/1000 CPS	$n(f)_o = 17.3$ modes/1000 CPS

a. Results

In both cases the corrected value of the modal densities are in much closer agreement with the observed estimates.

It does appear that acceptable engineering estimates of the modal density of heavily laden panels (including stiffeners) can be realized if the longitudinal wave velocity of the panel (taken alone) can be adjusted by the estimated or measured stiffness and mass factors of the actual board.

5. MODAL OVERLAP ANALYSIS

We seek reasonable assurances that $n(f)_o$, the observed modal density, is approximately equal to the true modal density, $n(f)_{true}$. That is, within the frequency range of this study was there sufficient modal overlap to conceal more modes, than were observed?

If statistically, the average bandwidths of modes (e.g. bandwidth at the 3 db down points) approaches the modal separation, $\frac{1}{n(f)}$, then modal overlap should occur and $n(f)_o$ should be less than $n(f)_{true}$. Restating, when $\frac{1}{n(f)} = \Delta b$ we should expect that on the average $n(f)_o$ would be approximately one-half of $n(f)_{true}$ — in any case, less than the $n(f)_{true}$. This is illustrated in Figure 6.

We examine the region of the frequency spectrum at which this might occur. From Reference 2

$$\Delta f = \frac{1}{n(f)}$$

let the modal separation, Δf, be equal to the modal bandwidth, Δb

$$\Delta f = \frac{1}{n(f)_{true}} = \Delta b \tag{8}$$

where,

$$\Delta b = \frac{f_n}{Q} \quad \text{and} \quad Q = \frac{1}{\eta}$$

substituting Δb into Equation 8 and $\frac{1}{\eta}$ for Q we obtain;

$$f_n = \frac{1}{\eta \, , n(f)_{true}} \tag{9}$$

where f_n is the frequency above which modal blending is pronounced.

a. Results

A review of the Δb's obtained from the vibration records show that over the vibration range the modal bandwidths (as measured by the analyzer) were on the whole less than the observed or computed modal separation.

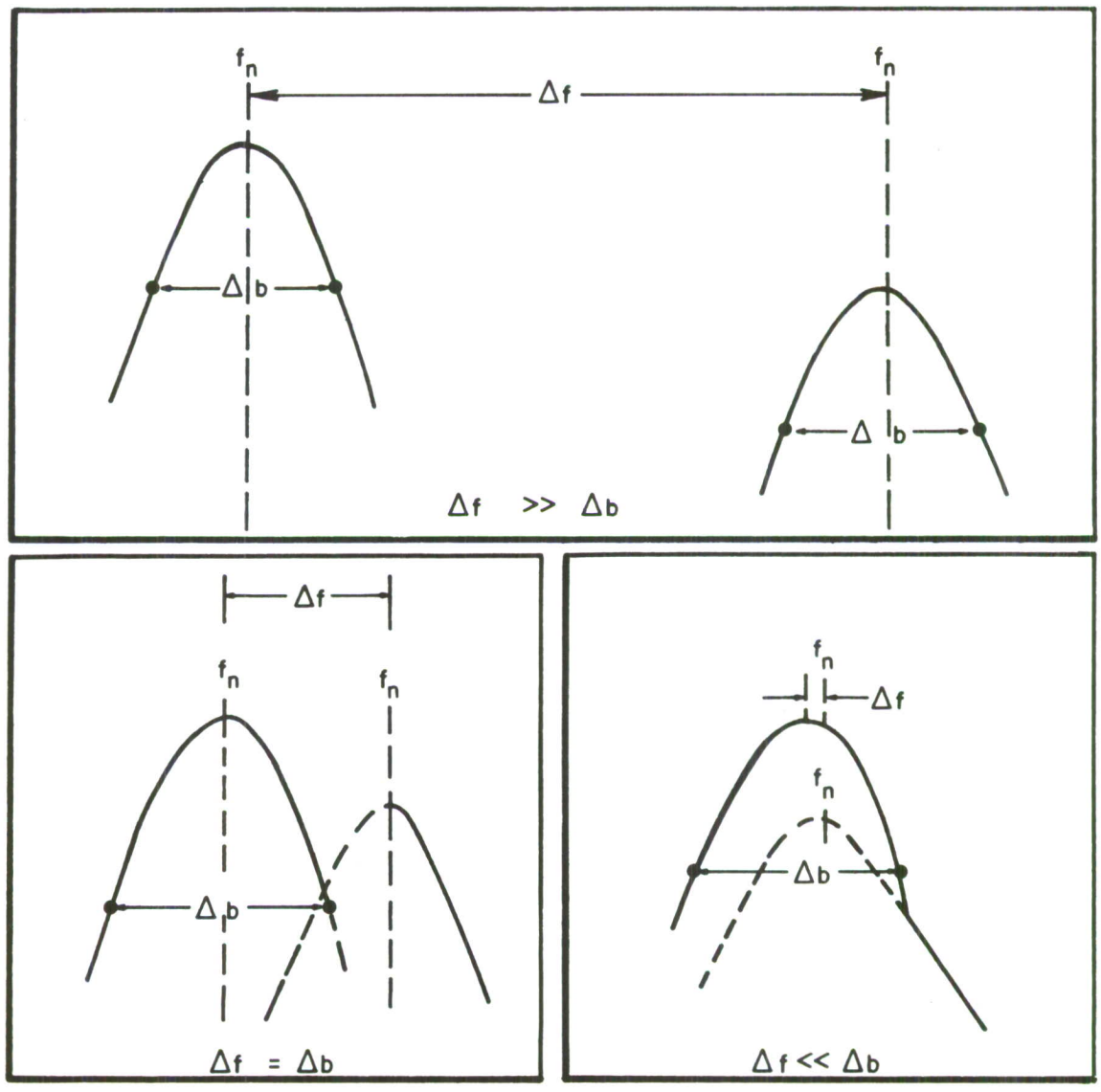

Figure 6. Modal Separation and Blending

For example:

Recalling that, $\Delta f_o = \frac{1}{n(f)_o}$; we compare modal separation to response bandwidths

	Δf_o	Δb_o
Board A	83 CPS	from 6 to 60 CPS
Board B	59 CPS	from 4 to 58 CPS

These results indicate that relatively little blending of modes occur - and that $n(f)_o$ represents a reasonable estimate. The records tend to confirm this. On the whole, the modes are distinct and identifiable up to 2000 CPS. To estimate the frequency above which we would expect substantial overlap, we return to Equation 9

$$f_n \simeq \frac{1}{\eta \, n(f)_{true}} \quad ; \text{ setting } n(f)_{true} = n(f)_o$$

For board A

$$n(f)_o = 0.012 \text{ modes/CPS}$$

and board B

$$n(f)_o = 0.017 \text{ modes/CPS}$$

It will be shown in Section IV and in Figure 13, that the loss factors of both boards at the higher frequencies (2000 CPS) tend to be independent of the frequency and approximately asymptotic. In our case it is approximately 2.0×10^{-2}.

Then,

$$f_{n_A} = \frac{100}{(2.0)(12)} \cdot 10^3 \sim 4200 \text{ CPS}$$

And,

$$f_{n_B} = \frac{100}{(2.0)(17)} \cdot 10^3 \sim 2900 \text{ CPS}$$

Of course, some modal overlap occurs even below 2000 CPS. Further, the overlap criterion of Equation 9 requires that the response magnitudes be sufficiently high to obtrude from the skirts of adjacent responses, thus modal overlap is also related to response magnitude.

b. Conclusions

Observed modal counts should, therefore, be considered as minimum values. It may be significant that in both cases the adjusted values of the modal density of the boards remain somewhat greater than the observed counts and that this difference represents occasional modal blending.

6. MODAL DENSITY OF OUTER PANELS

Modal responses of the panels were recorded through a 2 CPS filter. Three different locations on each face of the box were recorded. These mode counts were averaged per panel and then averaged for six panels to provide a total mean mode count for the box cover. In these experiments one small high frequency shaker (MB 1250) became available. The shaker was attached to a side panel of the box and remained in this location throughout the recording.

a. Results

Cumulative modes from the small shaker experiments were plotted in Figures 7 and 8. For graphical clarity the data points of Figure 7 are omitted. The cumulative mode plot is shown as a smoothed curve with a positively decreasing slope above, approximately 300 CPS. Figure 8 represents the expansion of Figure 7 in the low frequency range. The details of the expansion emphasize the difficulty of determining the modal density when modal blending is encountered. Below 300 CPS, the cumulative mode history is reasonably linear and behaves acceptably. But above this range, the observed slope $n(f)_o$ decreases; giving slope values approximately one-half that of the initial observation.

Examination of the vibration records showed a distinct trend of modal overlap above approximately 500 CPS — this is illustrated by samples (a), (b), and (c) of Figure 9. The certainty of questionable modes, indicated with arrows on (b) and (c), was verified by inspection of other accelerometer records which usually presented these obscured modes in much more distinct form. In fact, the multiple record method was used extensively when such doubts arose.

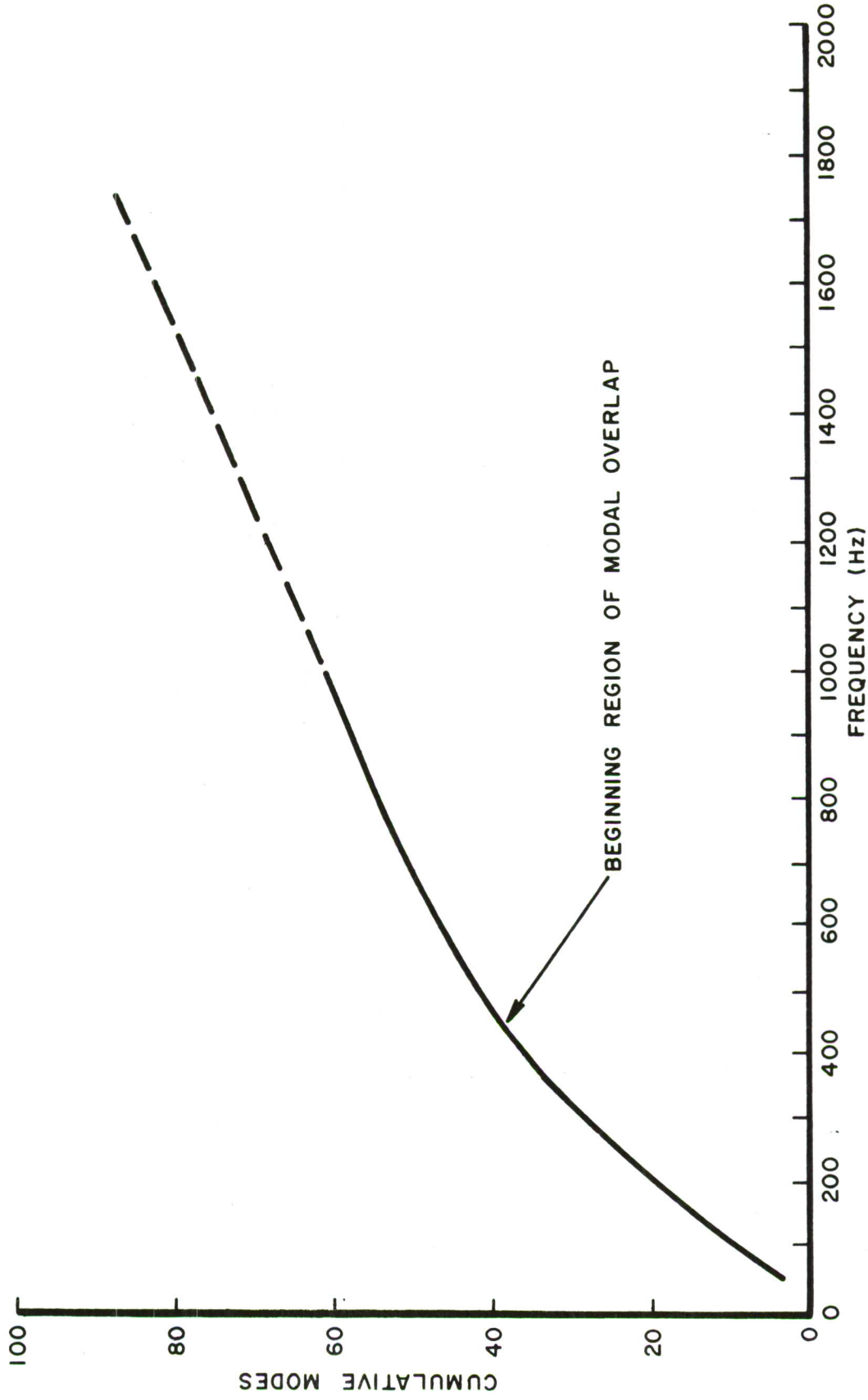

Figure 7. Mode Density of Cover Panels Showing Effect of Modal Overlap

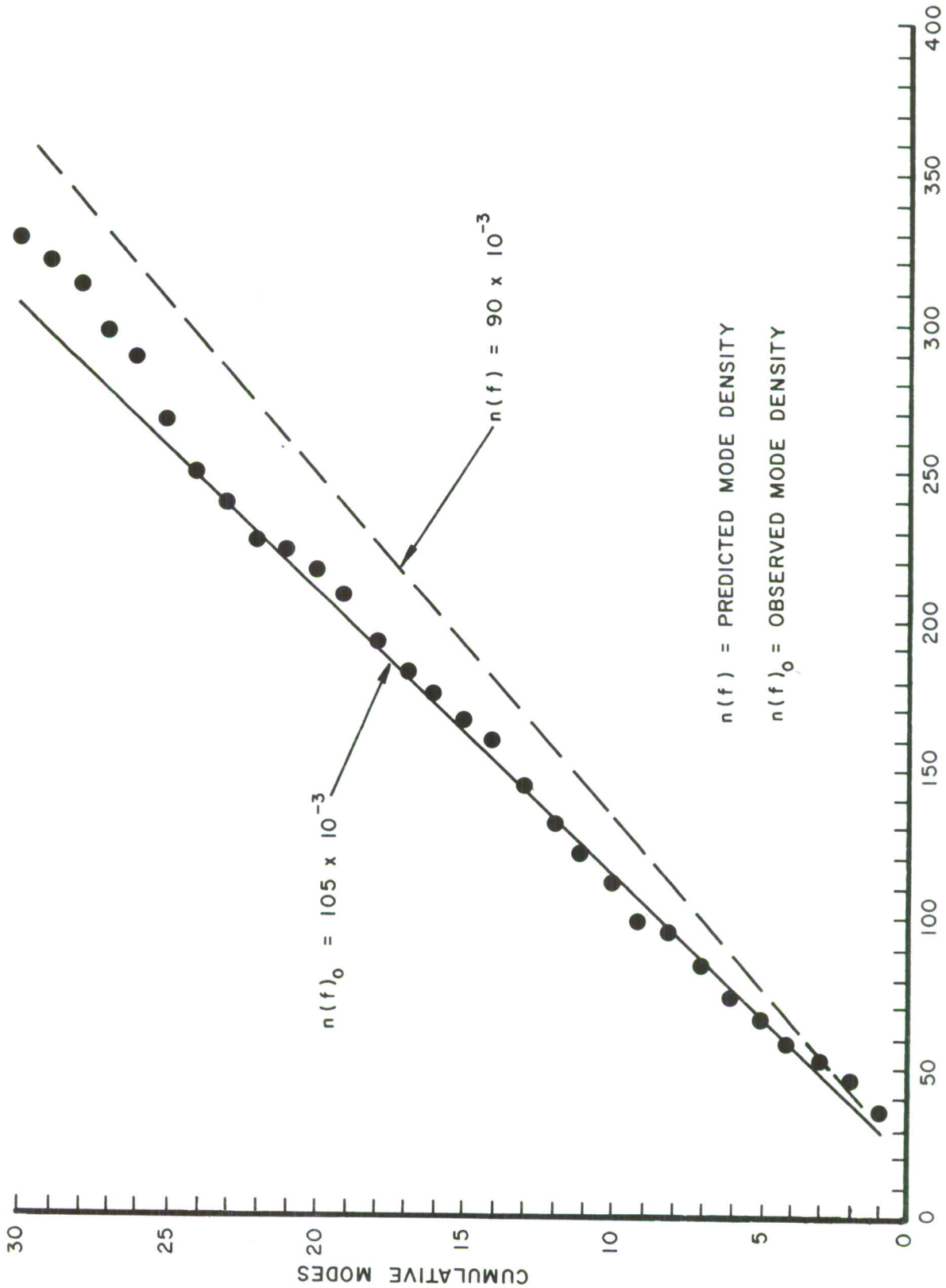

Figure 8. Mode Density of Panels Below Overlap Region

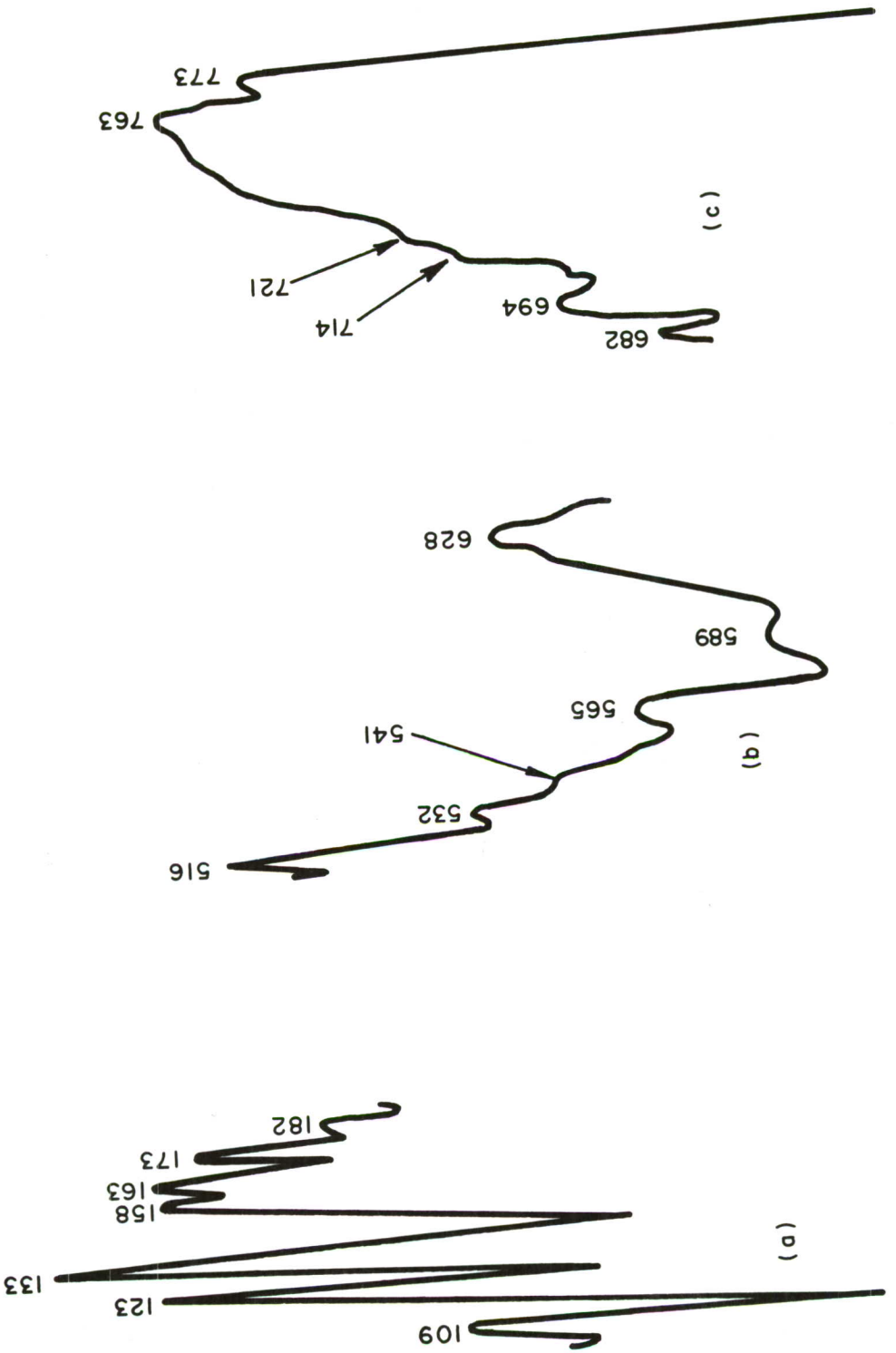

Figure 9. Typical Modal Responses Showing Increasing Modal Overlap Vs. Frequency

It is seen then that the decreasing slope above 500 CPS is due to the modal sharing process and that the initial slope rather than the final slope represents the most accurate estimate of the modal density.

As in the case of the printed circuit boards, one might estimate the modal density box cover from the expression,

$$n(f) = \frac{\sqrt{3}}{C_L\, t} A_p \cdot$$

This would be a minimum value due to the contributions from mechanical coupling through and to the printed circuit boards. Thus, the actual mode density should yield an observed $n(f)_o$ greater than the theoretical estimate, n(f). We investigate this returning to the modal density expression, where, for aluminum, C_L = 200,000 in/sec, t = panel thickness (.065 inches) and A_p is the area of the panels. We have in tabulated form:

	Length x Width (in)	Area (in^2)	n(f)
Top and bottom panel	15.375 x 9.75 x 2	149.91 x 2	39.90
Side panel (1)	15.375 x 7.50	115.32	15.35
End panel (2)	7.50 x 9.75 x 2	73.13 x 2	19.46
Cover panel (1)	15.25 x 7.50	114.38	15.22
		Total Theoretical n(f) =	89.93×10^{3}

The observed modal density of the panels should then be at least 90×10^{-3}. Examination of the slope of Figure 8 shows an $n(f)_o$ of 105×10^{-3} in rather close agreement with n(f).

b. Conclusions

The initial slope of the accumulative mode curve for the box cover represents the most accurate estimate of the mode density.

The mode density of the cover panels is in good agreement with the theoretical expectation; being slightly less but approximately equal to the observed value.

7. SUMMED MODAL DENSITY OF BOARDS

Ultimately, we are concerned with the boards not as individual, disconnected energy sinks but rather as a two-column parallel array of boards having a total mode density equal to the sum of the individual boards — this is the meaning of element two of our chosen model; the two element energy sharing structure. Therefore, to obtain $n_2(\omega)$ of Equation 2 we add the board modal densities; observing that for like boards we may obtain the totals in proportion to their areas.

Summing the mode densities of the boards, we have 4 boards of type A and 3 of the type B, also three smaller boards similar to type A and totaling 1.45 times the area of a type A board.

$$
\begin{aligned}
n(f)_o \text{ of A} &= 4 \times 12.0 &&= 48.0 \times 10^{-3} \\
n(f)_o \text{ of small boards} &= 1.45(12.0) &&= 16.4 \times 10^{-3} \\
n(f)_o \text{ of B} &= 3 \times 17.3 &&= 51.9 \times 10^{-3} \\
&\qquad \text{Total } n(f)_o &&= 116.3 \times 10^{-3}
\end{aligned}
$$

Here, we have used the observed board densities but we could just as easily have substituted the adjusted values, $n(f)'$. This would result in a total of 119×10^{-3} — an insignificant difference representing about two percent.

In retrospect, we note that the predicted modal density of the box cover is about 90×10^{-3}, being approximately equal to that of the board assembly. Later on (Sections IV and V) we will set $n_1(f) = n_2(f)$, obtaining small error and gaining some manipulative advantage as a result. It should be stressed that it is not necessary that this near equality exist — it simply happens to be so, in this case.

8. MODAL PATTERNS OF BOARDS A AND B

After mode density measurements had been taken in the test jig, each board was sprinkled lightly with fine Ottowa sand and modal patterns and their frequencies were recorded (Figures 10 and 11).

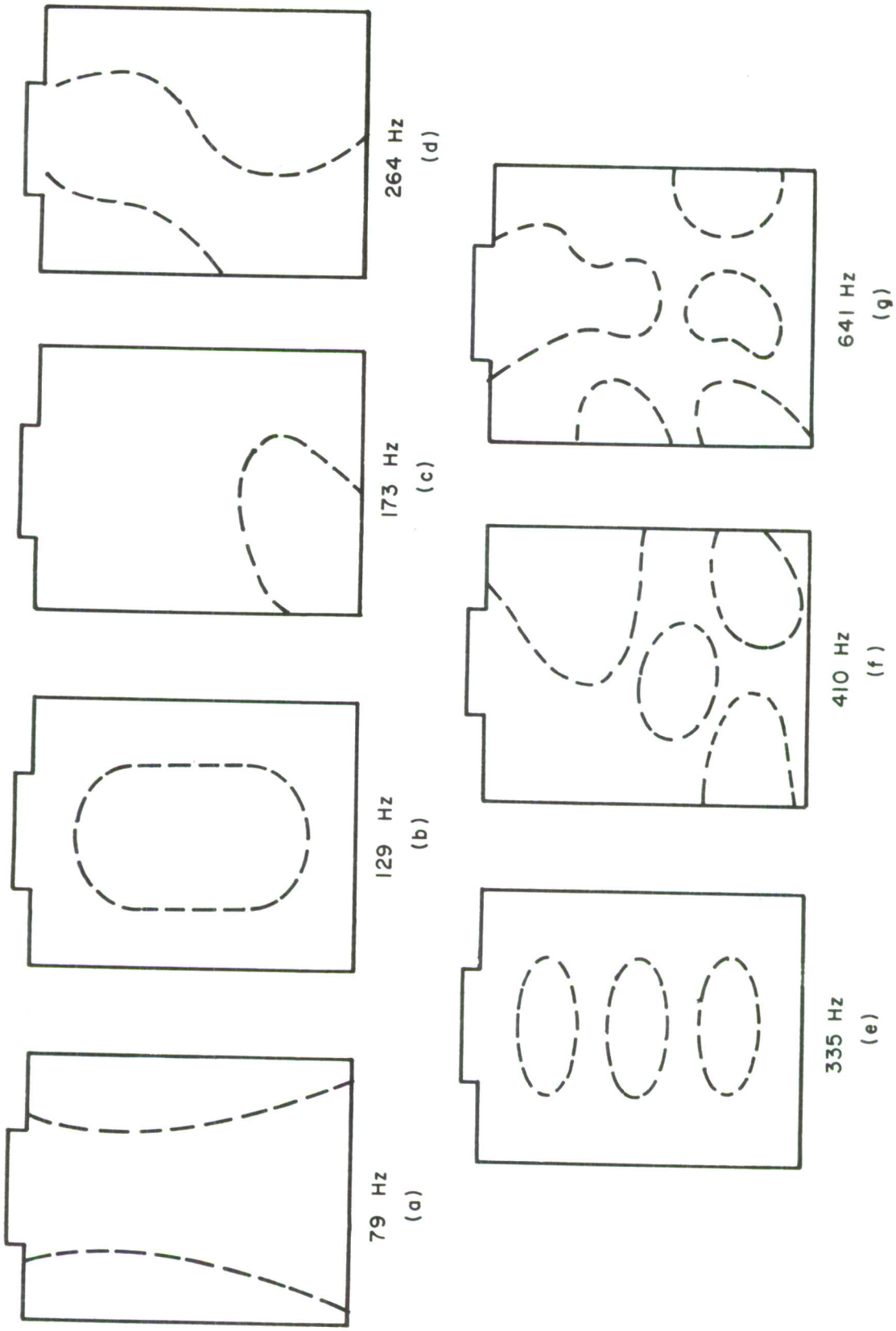

Figure 10. Modal Patterns of Printed Circuit Board A

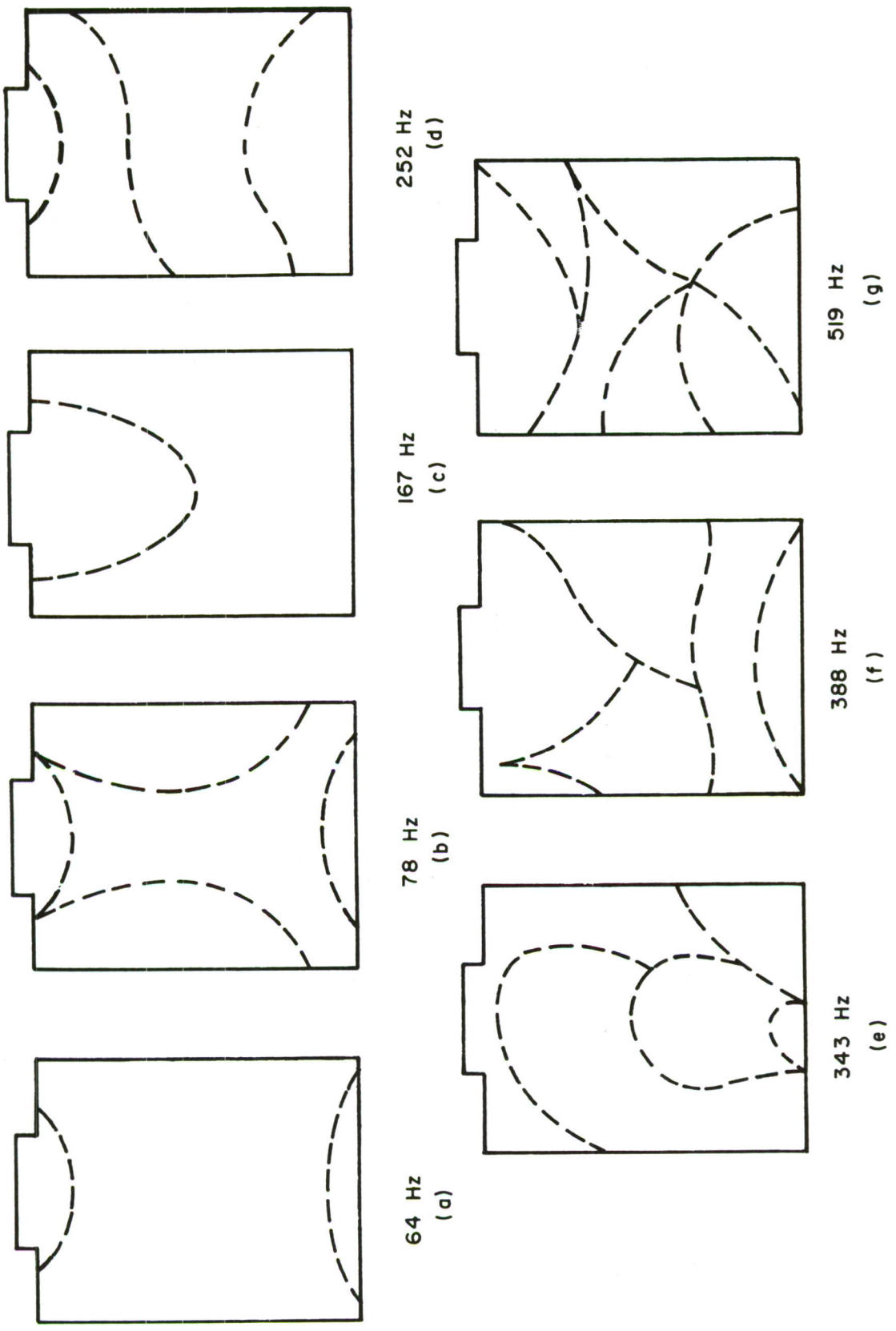

Figure 11. Modal Patterns of Printed Circuit Board B

a. Results

As might be expected, the modal patterns at low frequencies do not show a close relationship to mode shapes based upon classical boundary constraints and plate modal theory. For example, (b) of Figure 10 exhibits a modal pattern reminiscent to the first mode of a fully clamped plate but (a) of the same figure shows a modal pattern similar to the fourth mode of a cantilever plate. Observation seems to confirm this latter, capricious behavior. During this mode (79 CPS) the plug-in (tongue) end of the board tended to displace against the spring contacts of the mating connector, in a manner resembling a cantilevered response.

At 335 CPS the modal pattern appears to develop into a more regular form, say characteristic of the third mode of a hinged-hinged plate. We explore this possibility by examining the modal equation for plates. The number of modes of a simply supported plate whose orthogonal frequencies $(\omega)_{mn}$ are less than a specified frequency, ω, is given by (Reference 3):

$$N_{(\omega_{mn} < \omega)} = \frac{1}{4\pi}\left[A_p\left(\frac{\omega}{c}\right)^2 - P\left(\frac{\omega}{c}\right) + \pi\right] \qquad (10)$$

This expression has a quadratic solution shown in Appendix III.

Setting, N = 3 and solving for the frequency (Appendix III) we obtain f = 367 CPS. This value is in rough agreement with the observed frequency. However, the results also state that below 367 CPS, board A contains three mode patterns. Examination of Figure 10 shows that there are at least five modal patterns present. Continuing, we set N = 1. Here, the frequency solution for only one mode would be an estimate of the first, or fundamental frequency. Proceeding as before, we obtain f = 214 CPS. There is no agreement with the observed modal patterns — and, as before, we note that below 214 CPS there are at least three other patterns. Modified forms of Equation 10 accounting for other boundary conditions were similarly investigated — the agreement was no better and the observed modes always greatly exceeded theoretical predictions.

b. Conclusions

We are now able to account for the peculiar "bunching" behavior of the cumulative mode count at the low frequency extremity of the curves of Figures 4 and 5. It is evident from the modal behavior patterns of Figures 10 and 11 that the increasing modal density at this portion of the curve is due largely to real and variable boundary conditions and to the component influences which result in the generation of more low frequency modes than the predictive theory of Equation 10 permits.

It is probable that most equipment configurations of this sort will exhibit like behavior and, in the future, it should prove profitable to subject other plug-in boards to similar studies.

Finally, it is instructive to note that care should be exercised (when determining modal densities via the slope method) to insure that the slope line is drawn above the bunched region of the curve and below the region of modal blending; if an accurate estimate of the modal density is to be realized.

SECTION IV
LOSS AND COUPLING FACTORS

1. LOSS FACTOR MEASURABLES

Certain classes of loss factors must be determined before the coupling factor can be described. In Reference 2 we note that for a two element energy sharing structure we have two, interrelated expressions:

$$\eta_{1a} = \eta_1 + \frac{\eta_{12}\ \eta_2}{\eta_{21} + \eta_2} \tag{11}$$

$$\eta_{2a} = \eta_2 + \frac{\eta_{21}\ \eta_1}{\eta_{12} + \eta_1} \tag{12}$$

Where η_{1a} and η_{2a} are the apparent dissipation loss factors of the box cover and circuit boards as measured in their normal, interconnected state, and η_1 and η_2 are the true dissipation loss factors, respectively, of the outer cover as measured without the presence of the boards, and of the boards as measured without the presence of the cover.

From the above expressions, we must obtain η_{21} so that we can define the coupling factor,

$$\mu_1^2 = \frac{\eta_{21}}{\eta_{21} + \eta_2}$$

Selecting Equation 11, noting from Reference 1 that $\eta_{12}\, N_1 = \eta_{21}\, N_2$ and solving for η_{21}, we have:

$$\eta_{21} = \frac{\eta_1\ \eta_2 - \eta_{1a}\ \eta_2}{\eta_{1a} - \eta_1 - \frac{N_2}{N_1}\,\eta_2} \tag{13}$$

Also, since $N_1 = n_1(f) \cdot \Delta f$ and $N_2 = n_2(f) \cdot \Delta f$, we substitute in the above expression and obtain:

$$\eta_{21} = \frac{\eta_1\ \eta_2 - \eta_{1a}\ \eta_2}{\eta_{1a} - \eta_1 - \frac{n_2(f)}{n_1(f)}\ \eta_2} \tag{14}$$

We have seen earlier that the total modal density of the circuit boards is very nearly equal to the total modal density of the cover.

Allowing this assumption results in a slight change of η_{21} and an almost imperceptible influence on μ_1^2, which is of ultimate importance. Also, the effect on the prediction Equation 2 is small — amounting to less than 1.5 db. Thus, we set

$$\frac{n_2(f)}{n_1(f)} = 1.$$

As a consequence, we are permitted to set $\eta_{2a} \approx \eta_2$. Substituting these conclusions into Equation 14, we obtain:

$$\eta_{21} = \frac{\eta_1 \eta_{2a} - \eta_{1a} \eta_{2a}}{\eta_{1a} - \eta_1 - \eta_{2a}} \tag{15}$$

This final expression now contains those loss factors which can be measured with the exception of η_1, which will be discussed later.

The same recordings used for determining the modal densities also provided measurements of the Q and its inverse, η. The loss factors, determined by the half power point method, were arithmetically averaged over 1/3 octave intervals. Measurements extended to approximately 2 KHZ.

The loss factor for the boards was measured for two conditions: a loss factor obtained with the boards mounted in the equipment box (in situ) and a loss factor obtained with the board mounted in the test fixture (Figure 12). Two other plots were provided: one, (Figure 13) of the in situ loss factor, η_{2a}, plotted together with an η_{2a} of circuit boards measured by another investigator (Reference 6) during studies of an Atlas guidance computer (the second (Figure 14) a plot of the box cover mean apparent loss factor, η_{1a}).

The Atlas computer, η_{2a}, exhibits much wider scatter than the equipment η_{2a}, perhaps because of insufficient averaging of modes within the 1/3 octave bandwidths. Nonetheless, both loss factors are in the same range and seem to follow much the same inverse trend with frequency. A significant and useful

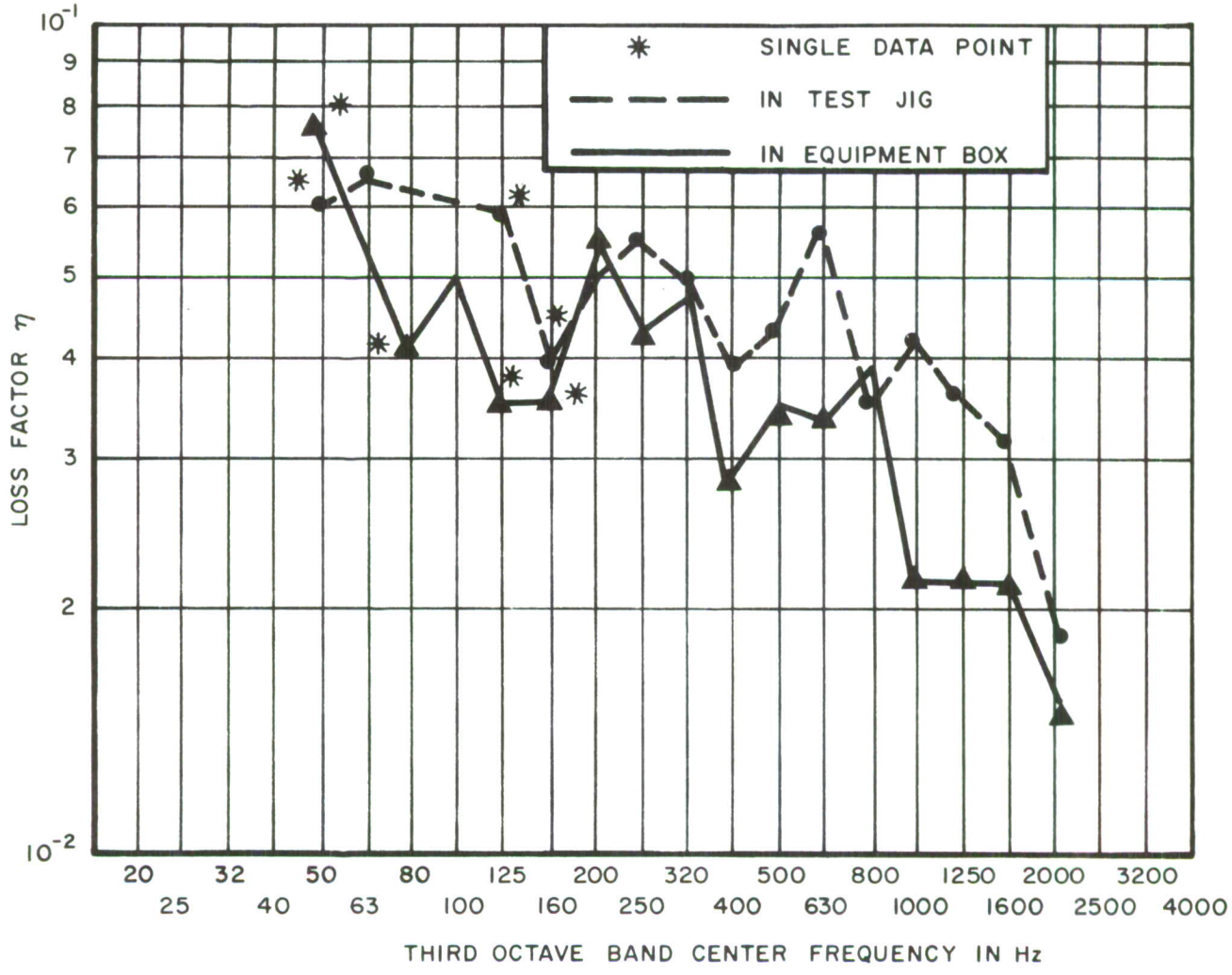

Figure 12. Comparison of Circuit Board Loss Factors When Mounted in Test Jig and Then in Situ

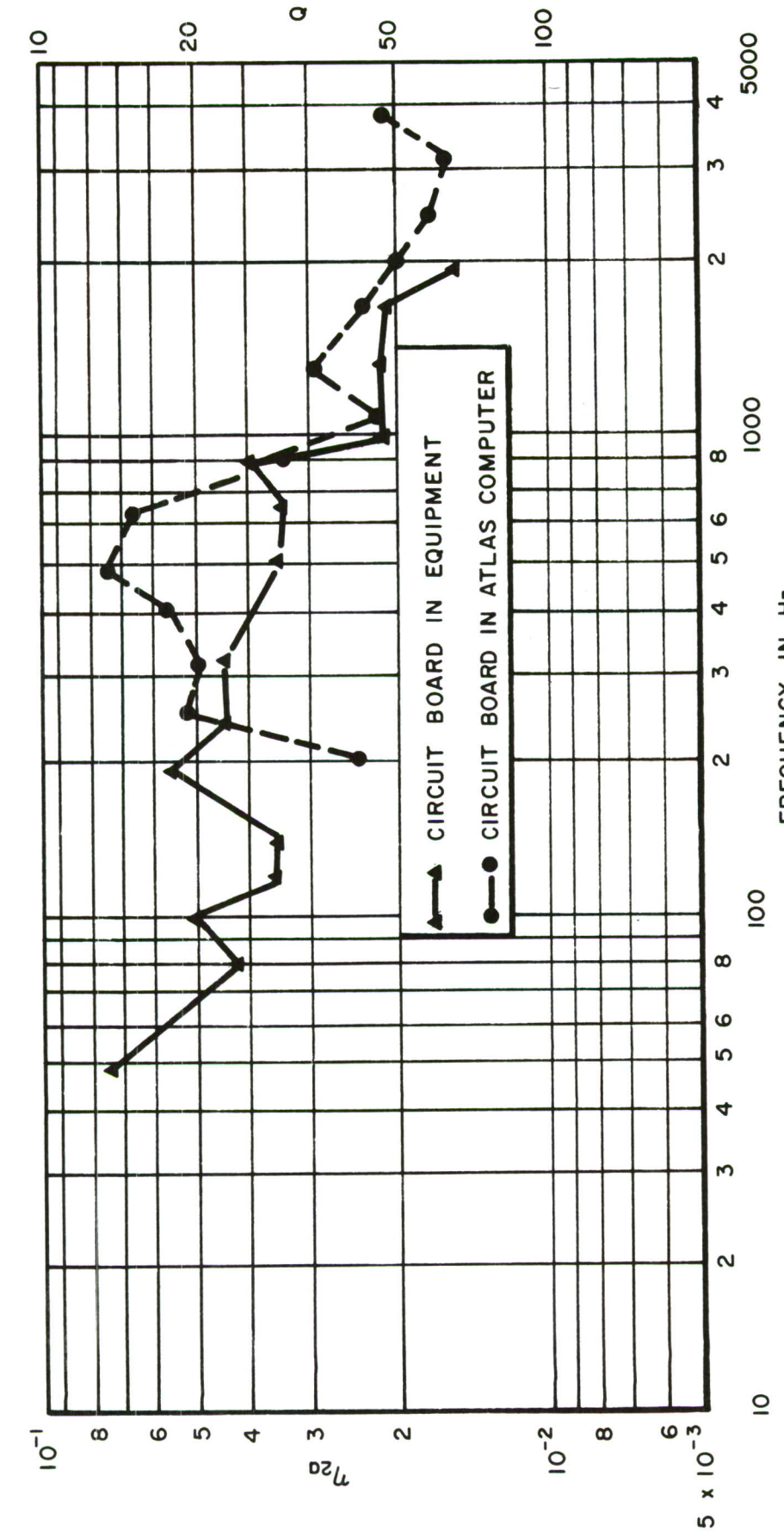

Figure 13. Apparent Loss Factor η_{1a} for Circuit Board Mounted in Atlas Computer Compared to the Equipment Board

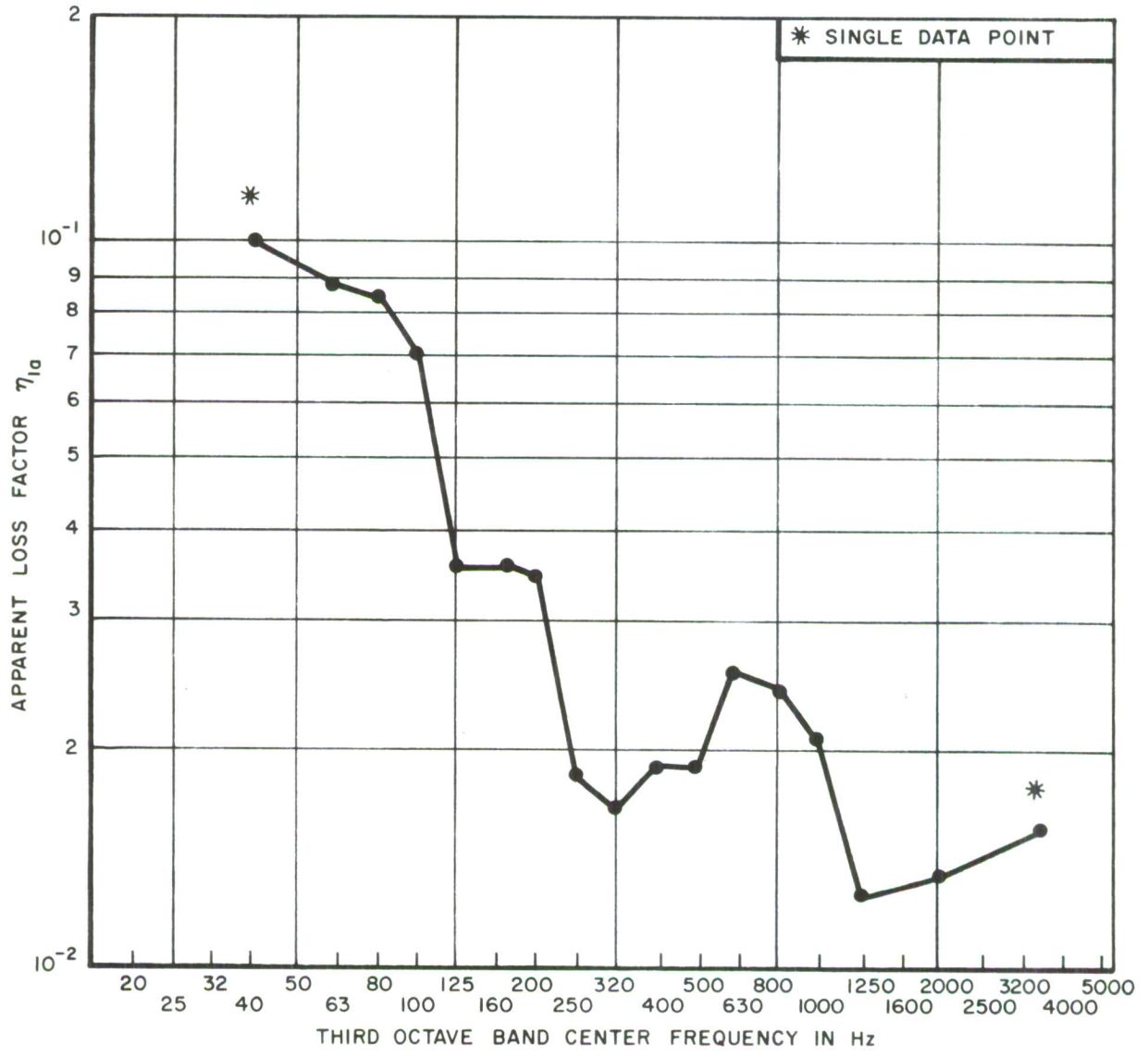

Figure 14. Mean Apparent Loss Factor η_{1a} of Equipment Cover

conclusion arises from the examination of Figure 12. Note that the loss factor of the board, when mounted in the jig, seems to change very little when mounted in situ. It is this observation that permits us to set $\eta_2 \approx \eta_{2a}$, as described earlier.

2. OBTAINING THE TRUE LOSS FACTOR OF THE COVER, η_1

Data had not been obtained of the true loss factor of the cover η_1, however, other investigators had recorded the reverberation time versus frequency history of an empty box of the same material, thickness and of similar size, shape, and construction.

Since $\eta_1 = \frac{2.2}{fT_s}$ where f is the 1/3 octave center frequency and T_s is the 60 db decay time, we are able to plot η_1 and include it with η_{2a} and η_{1a}. This is shown in Figure 15.

3. COMPUTING η_{21} AND μ_1^2

The three curves are then represented as being approximately a straight line, log-log, negatively sloping function that are asymptotic on both ends of the frequency spectrum (Figure 16). The asymptotes result from an examination of the trend of the data and of similar data from other investigators. Since the measurements extend to only 2000 CPS, dashed lines are provided to indicate extrapolation beyond this limit for values of η_{2a} and η_{1a}.

Returning to Equation 15, η_{21} is calculated and plotted and the results are shown in Figure 17. A plot of an η_{21} of the Atlas computer (Reference 6) is included for comparison.

The two coupling loss factors do not agree in magnitude and trend — they diverge, noticeably, above 2 KHZ.

4. ENERGY COUPLING FACTOR μ_1^2

With η_{21} and η_{2a} defined, we plot μ_1^2 as shown in Figure 18. The curve exhibits interesting properties. Recalling that $T_1 \mu_1^2 = T_2$ where T_1 and T_2 are the modal vibration energies of the cover and boards respectively, we note

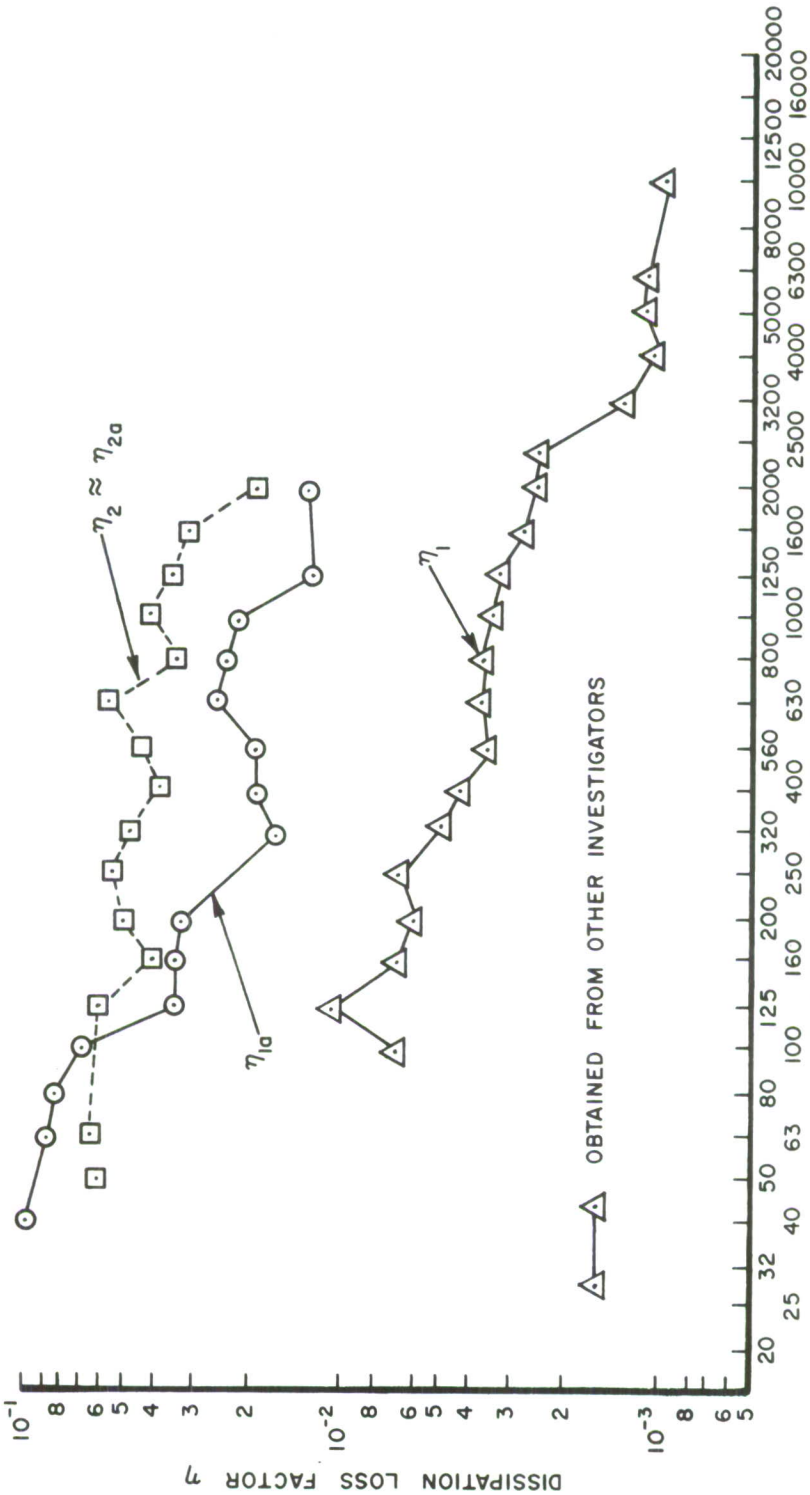

Figure 15. Plots of Dissipation Loss Factor for Boards, η_{2a}, η_2 and Equipment Cover, η_{1a}, η_1

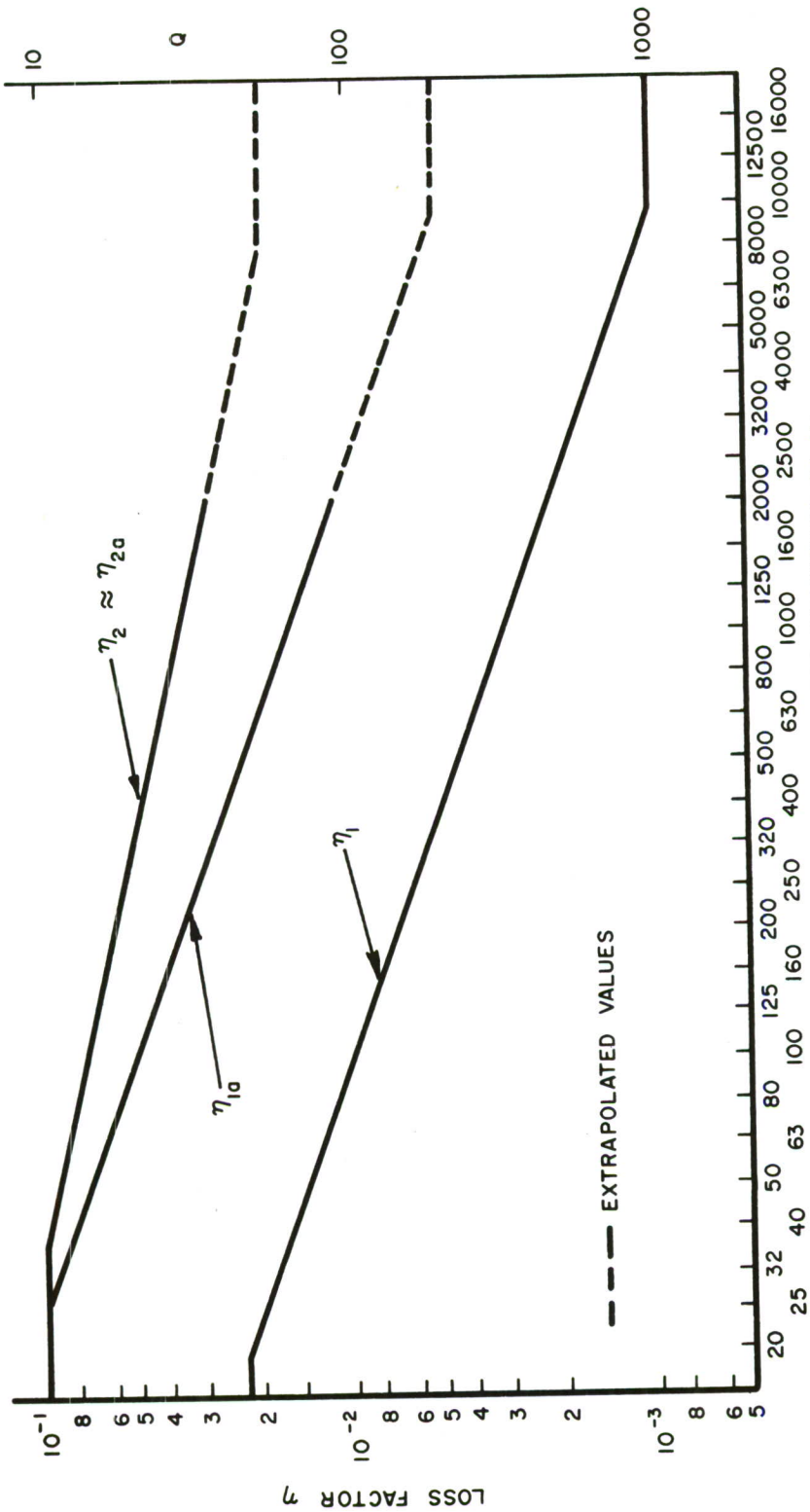

Figure 16. Smoothed Forms of Dissipation Loss Factors Used to Determine η_{21}

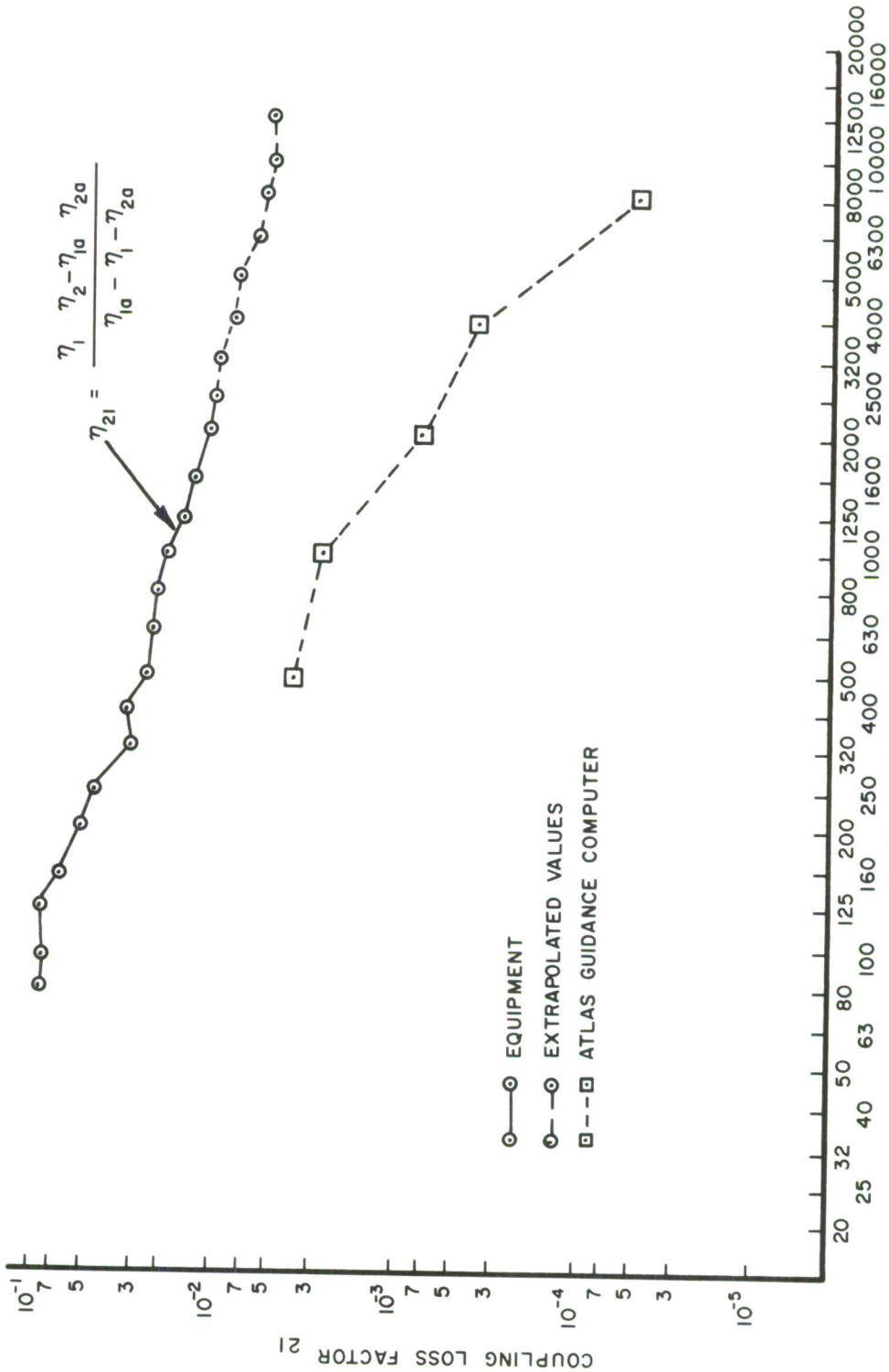

Figure 17. Coupling Loss Factor as Determined From Loss Factors of η_1, η_{1a}, η_{2a} and Compared to Values Determined by Other Investigators

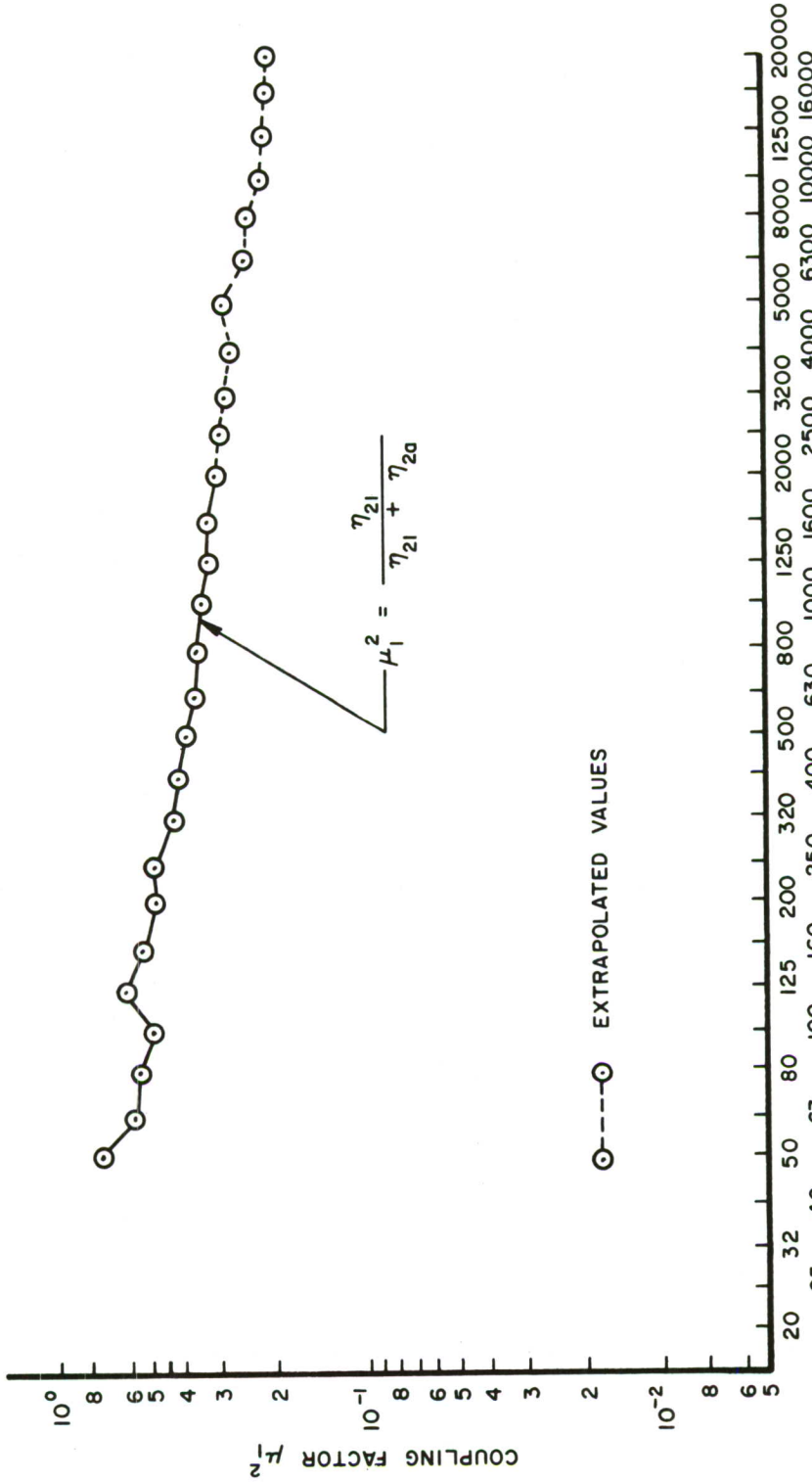

Figure 18. Energy Coupling Factor, μ_1^2 (Box Cover to Printed Circuit Boards)

that μ_1^2 has a gradual negative slope of approximately 1.2 db/octave. The curve indicates that the printed circuit boards are behaving essentially as a broad-band vibration receiver (that is, with respect to their energy source, the cover).

SECTION V
VIBRATION PREDICTION

1. PREDICTION AND MEASUREMENT

Restating Equation 2 we have:

$$\langle S(\omega)_2 \rangle = \langle S(\omega)_1 \rangle \frac{n_2(\omega) m_1}{n_1(\omega) m_2} \mu_1^2$$

m_2 is obtained by weighing the removed printed circuit boards, and amounts to 7.88 pounds. The remainder, m_1, is 9.50 pounds. The ratio m_1/m_2 is equal to 1.22, or 1.7 db ($20 \log_{10}$). Since

$$\frac{n_2(\omega)}{n_1(\omega)} = 1$$

Equation 2 becomes:

$$\langle S(\omega)_2 \rangle = \langle S(\omega)_1 \rangle \; 1.22 \; \mu_1^2 \qquad (16)$$

We will record our noise spectral values of grms ($\bar{g}$) over 1/3 octave bandwidths, thus Equation 16 is expressed as:

$$\langle \bar{g}(\omega)_2 \rangle = \langle \bar{g}(\omega)_1 \rangle \left[1.22 \; \mu_1^2 \right]^{\frac{1}{2}} \qquad (17)$$

or, in db form:

$$20 \log_{10} \langle \bar{g}(\omega)_2 \rangle = 20 \log_{10} \langle \bar{g}(\omega)_1 \rangle + 0.9 \text{ db} + 10 \log \mu_1^2$$

Two small high frequency shakers were attached to opposite sides of the box cover (Figures 19 and 20). A random noise signal was passed through a B & K 1612 S/2 spectrum shaper, and from there to the shaker amplifiers. Therefore, the shakers were operating in parallel with respect to spectral shaping.

Two accelerometers (Clevite 2E1) were located on the two opposite and largest panels of the box. These were designated panels one and two. One Endevco 2222 accelerometer, mounted on each of three boards in the first column of boards (Type A), provided the response measurements for $\langle \bar{g}(\omega)_2 \rangle$. The two cover accelerometers provided a control for spectral shaping of the box cover. A curve was obtained to approximate a vibration response field

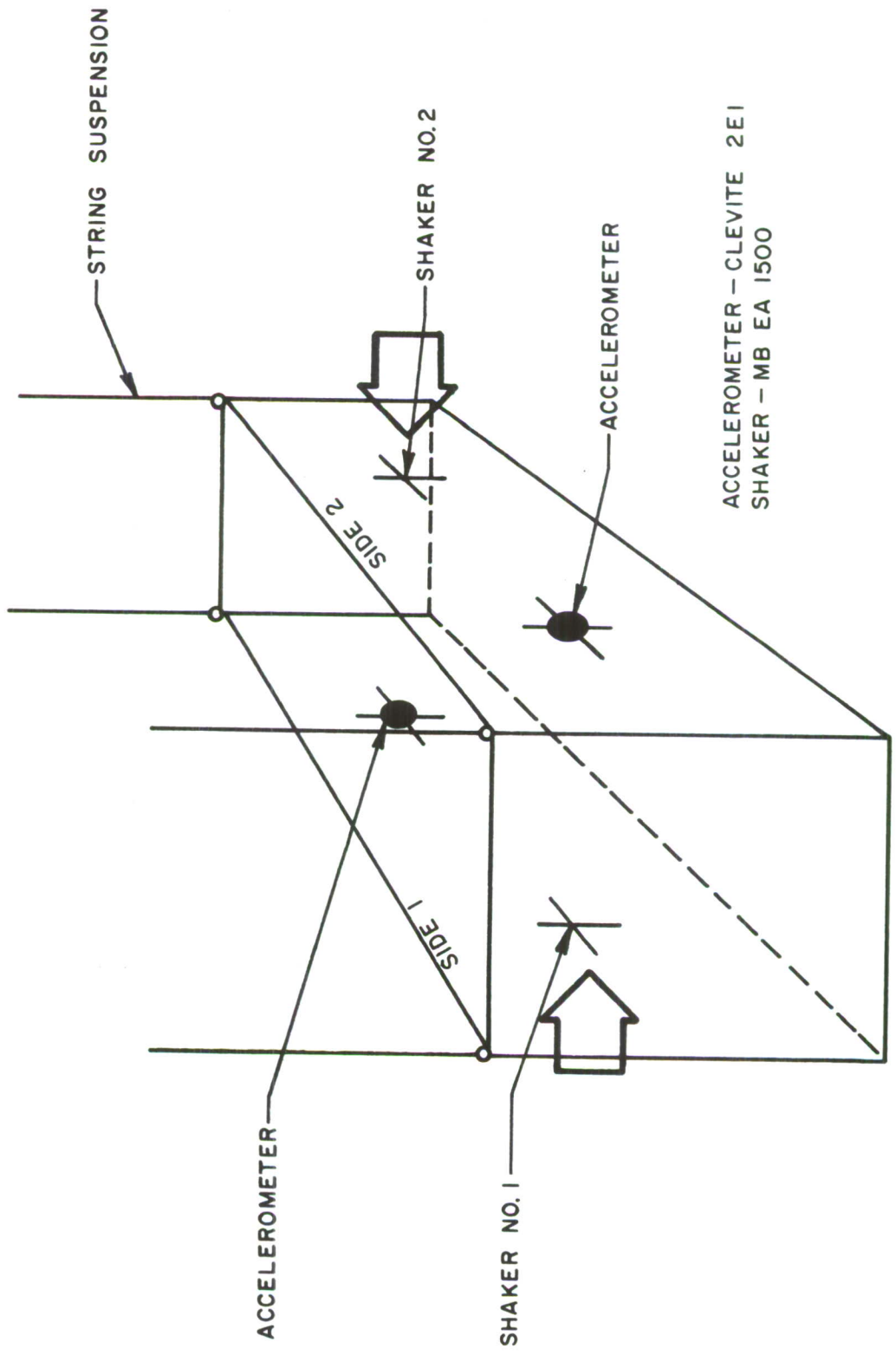

Figure 19. Shaker Arrangement and Accelerometer Locations for Measuring Vibration Level of Box Cover and Boards

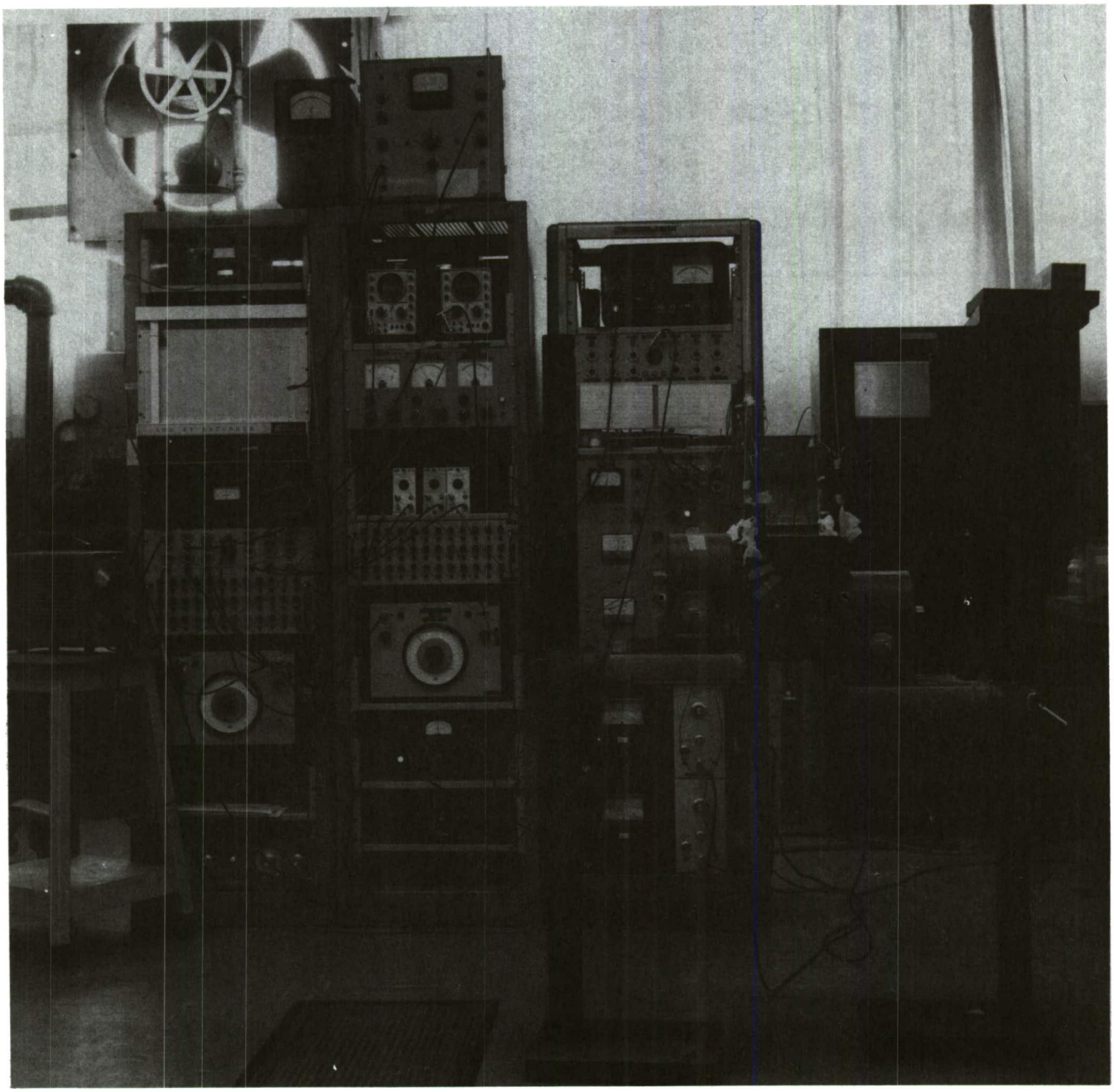

Figure 20. Shaker Arrangements and Accelerometer Locations for Measuring Vibration Levels of Box Cover

resulting from coupling to an acoustic source. One accelerometer was left in place after spectral shaping to provide a spectral control check, and the remaining accelerometer provided the roving pickup points for the box panel. Three points per panel were recorded in the 1/3 octave frequency intervals fro 40 Hz to 16 KHz, for a total of 18 samples.

During each data run on the box cover, one location of each of the three board accelerometers was similarly recorded. When the measurements on the three board locations were completed, the accelerometers were relocated to the three other boards located in the adjacent column of boards (Type B). Thus, there were also a total of 18 readings.

The results of each board were arithmetically averaged; then the three boards were in turn averaged. The Type B column of boards were similarly treated, and, finally, both board columns were averaged. This provided the spatial response average, $<\bar{g}(\omega)_2>$.

The same averaging procedure was applied to the accelerometer data from the box cover to obtain $<\bar{g}(\omega)_1>$, (Figure 21). As a final step, the cover vibration field, $<\bar{g}(\omega)_1>$, was substituted into Equation 17 and the predicted response field, $<\bar{g}(\omega)_2>$, was obtained. This field was compared to the measured value. Both are shown in Figure 22.

a. Results

The agreement between theory and measurement is surprisingly good, especially above 200 Hz. That the spread between observed and predicted values increases below this region is an expected result. This is because power flow between the ensembles of mode sets (in this case represented by 1/3 octave intervals) requires that a mode or modes exist, and rather uniformly so, in the ensemble interval. These conditions become less probable as the ensemble bandwidths decrease which in this case with the 1/3 octave resolution. This is in violation of the funadmental assumptions that permit use of the power flow equations.

Starting approximately one octave above the first modes of the board and box cover (approximately 200 Hz) the measured and predicted response values

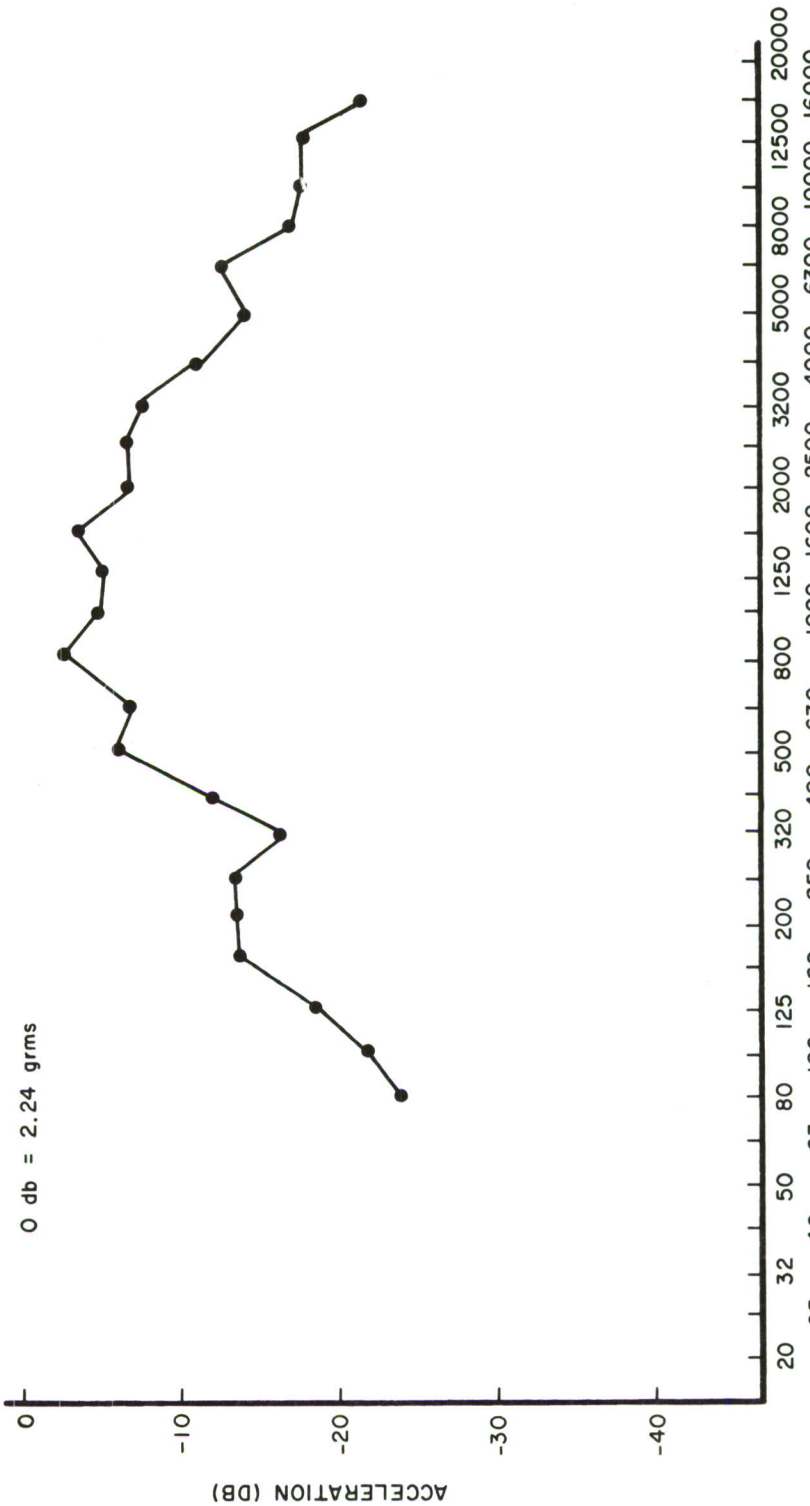

Figure 21. The Vibration Field of Equipment Cover Averaged Over Six Panels of Box

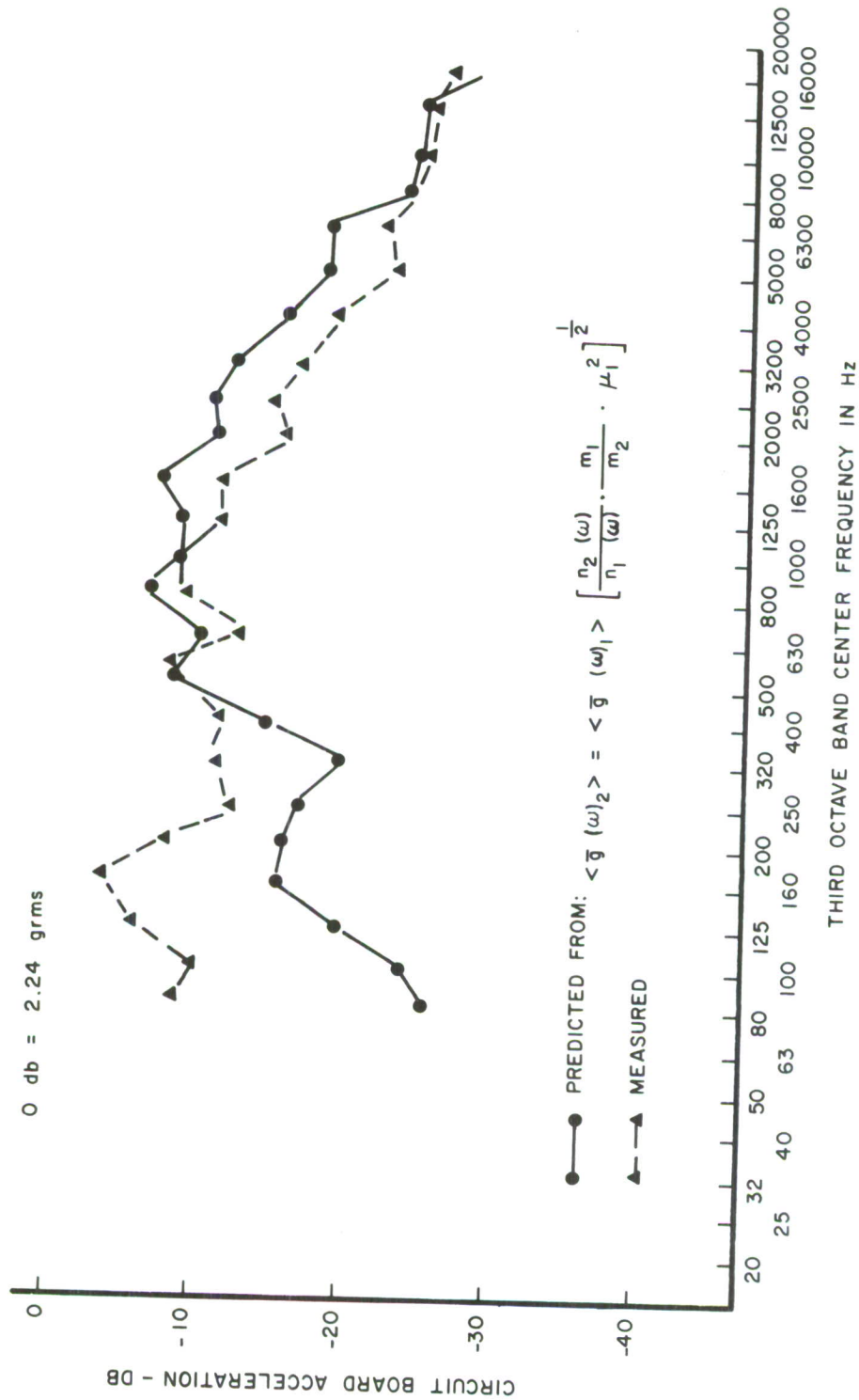

Figure 22. Comparison Between Circuit Board Response Measurements and Predicted Values

of the boards agree within about 3 db (average) and agreement extends over six octaves — an impressive demonstration of the utility potential and extensive coverage capabilities of the energy method.

b. Experimental μ_1^2

If we insert the measured values of $<\bar{g}(\omega)_1>$ and $<\bar{g}(\omega)_2>$ into Equation 17 we may then solve for μ_1^2, term it experimental, and compare this coupling factor to the previously derived form based on a two nodal model. This should give us some measure of the model validity, and should provide us with a useful comparison between experiment and theory.

c. Discussion

The two coupling factors are shown in Figure 23. Both curves agree in trend but the experimental μ_1^2 appears to be higher everywhere. Between 500 Hz and 5 KHz both appear to be on the average within 3 db of each other. There is a suggestion (below 8 KHz) that μ_1^2 should be somewhat steeper in slope than was obtained in the derived form. This, in turn, suggests that η_{21} should also decrease somewhat more sharply with frequency (Figure 18). At this point, it should be noted that the coupling loss factor, η_{21}, is a cumbersome expression, and is subject to considerable potential error.

Why the experimental coupling factor remains greater than μ derived, is not clear. Errors sttributable to the structural mass measurements and the mode density assumptions do not seem sufficiently large to account for a 3 db difference. Thus, our suspicion is reinforced that the basic form of η_{21} is at fault. However, much more detailed information concerning the nature and extent of errors accumulated during the derivation of η_{21} is required before this can be firmly concluded.

The most striking difference between the two curves appears at approximately 8 KHz. Here, μ_1^2 measured, rises rather abruptly and continues to do so up to 16 KHz. In previous works (Reference 2) it has been noted that at high frequencies, vibration of the boards in shear may result in a higher mode density than obtained for the board during bending at the lower frequencies. It

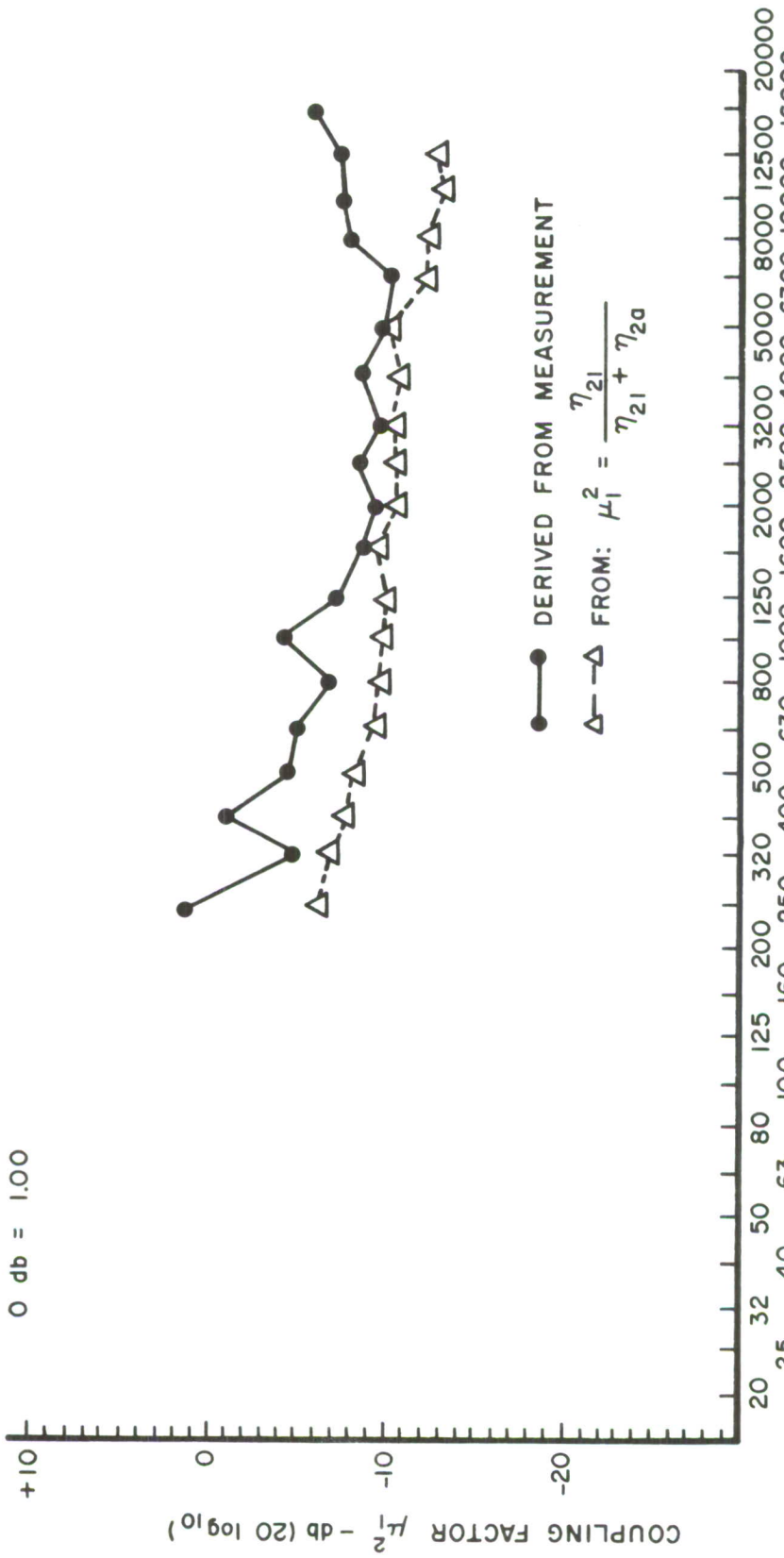

Figure 23. Comparison of Coupling Factor Determined by Experiment and by Theory

might be supposed that this would account for the behavior of μ_1^2 since by inspection of Equation 2 an increase in $\eta_2(f)$ would produce a proportionate increase in the mean square of the board response. However, computational checks indicate that noticeable shear contributions would occur above approximately 20 KHz. Thus, this explanation does not appear satisfactory. Apart from possible defects in the assumed model, it may be that torsion modal contributions from the bars and stringers (ignored in this study in order to simplify the model) may account for the observed increase. Again, future studies in this area should provide a more acceptable explanation.

If, in review, we consider the extensiveness of the input and response measurements and weigh them against the errors in the derivation of μ_1^2 then it seems prudent to consider the experimental value of μ_1^2 as representing the best estimate of the coupling factor — at least below 8 KHz.

Accordingly, a smoothed version of μ_1^2 (Figure 24) measured, is presented. The questionable region above 8 KHz is indicated by a dashed line.

It will be interesting to see, in the course of future studies and prediction efforts concerning similar equipment structures, whether or not this coupling factor will be sufficiently tractable for general use. In the interim, it is so proposed.

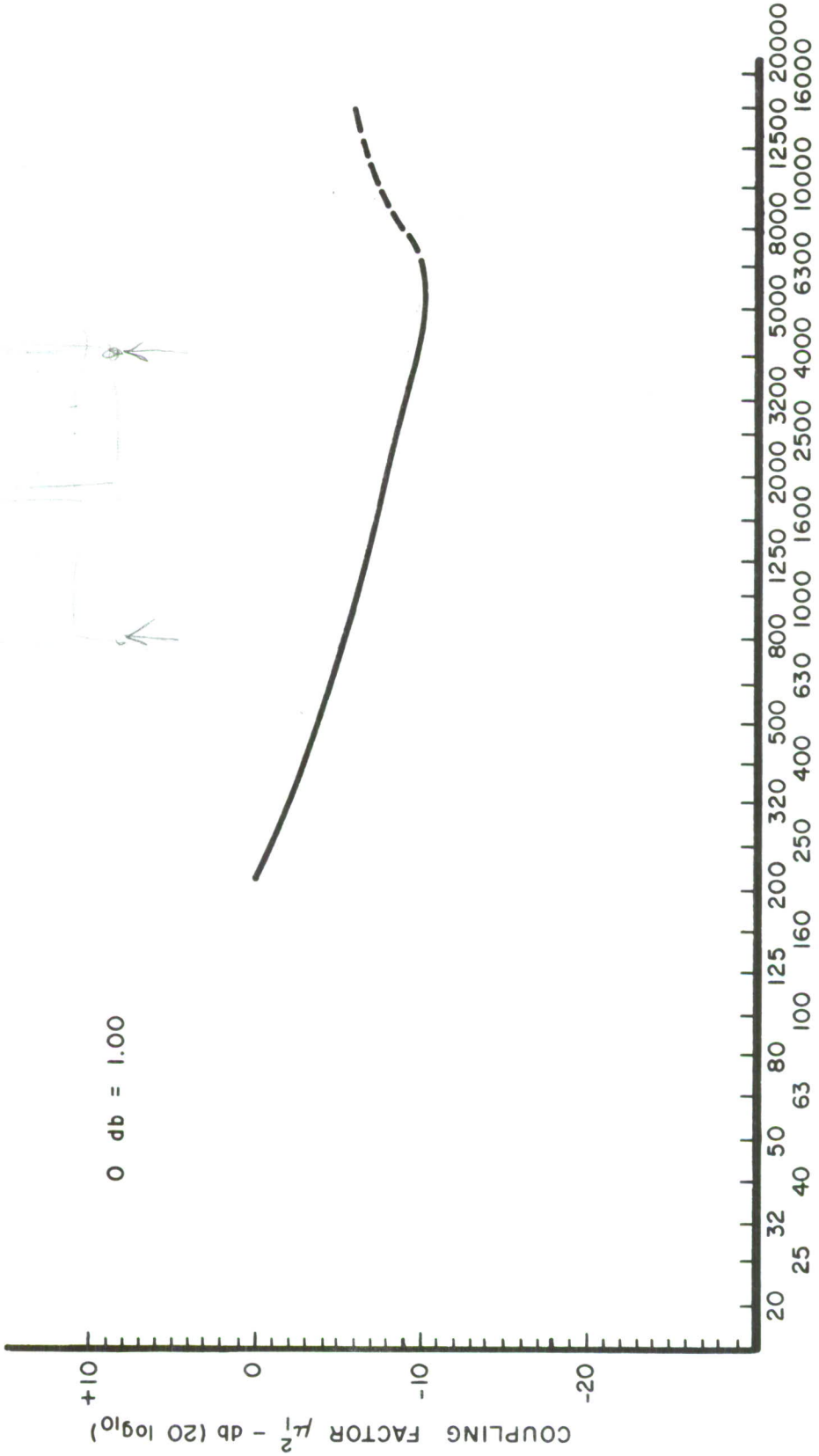

Figure 24. Final, Smoothed Form of μ_1^2 Determined from Measurements

SECTION VI
SUMMARY

1. CONCLUSIONS

The results of this investigation demonstrate that statistical energy methods may be effectively applied to at least certain classes of equipment, consisting of planar arrays enclosed by a cover, and can provide a useful prediction of the internal vibration levels over an extensive frequency range. It is further shown that such complex equipments may be represented as a two nodal system, thereby simplifying the prediction process. Other results show that modal densities of printed boards may be determined from thin plate theory and that acceptable engineering estimates may be realized by applying compensating procedures to account for mass and stiffness effects of heavily laden boards. Also in contrast to modal density estimates, it is demonstrated that the coupling loss factor is difficult to derive and can normally be determined only by indirect means.

A generalized coupling factor μ_1^2 is presented for application to those equipments having structural arrays and components that are considered similar to the equipment package studied in this work. Finally, it is proper to conclude that as future studies and measurements provide additional loss and coupling factors for more diverse classes of equipments; then it will be possible to effectively extend the application of energy method to more complex equipment and structures.

2. RECOMMENDATIONS

A follow-on study should be conducted to determine the coupling factor when the equipment box is directly excited by an acoustic source; for example, a reverberant chamber. If this step is successful, then it will be possible to predict the internal vibration of certain classes of equipment when exposed to reverberant acoustic sources.

If this phase is successful then, the way may open to simulate or reproduce the internal vibration levels of an equipment package by coupling small high

frequency shakers to the box surfaces; thereby providing low cost and flexible simulation of acoustic fields. If this technique proves feasible then a specification test method for equipments should be synthesized and included in MIL-STD-810(B).

REFERENCES

1. Eric E. Ungar, Fundamentals of Statistical Energy Analysis of Vibrating Systems, AFFDL-TR-66-52, May 1966.

2. D. U. Noiseux, R. H. Lyon, C. W. Dietrich, E. A. Starr, Bolt Bernaek & Newman, Dynamic Response, Energy Methods and Test Correlation of Flight Vehicle Equipments, AFFDL-TR-65-92, Vol I.

3. Manfred A. Heckl, Richard H. Lyon, Gideon Maindanik, Eric Ungar, New Approaches to Flight Vehicle Structural Vibration Analysis and Control, ASD-TDR-62-237, October 1962.

4. Denis U. Noiseux, Charles W. Dietrich, Ewald Eichler, Richard H. Lyon, Random Vibration Studies of Coupled Structures in Electronic Equipment, ASD-TDR-63-205, Vol. II, March 1964.

5. Harris and Crede, Shock and Vibration Handbook, McGraw-Hill, Inc., New York, 1961.

6. Bolt, Bernaek & Newman, Inc., "Measurement of Acoustic and Vibration Response of Atlas Guidance Computer," Report for American Bosch-Arma, Inc.

APPENDIX I

DETERMINATION OF MODE DENSITY FOR BOARDS WITH COMPONENTS AND STIFFENERS REMOVED

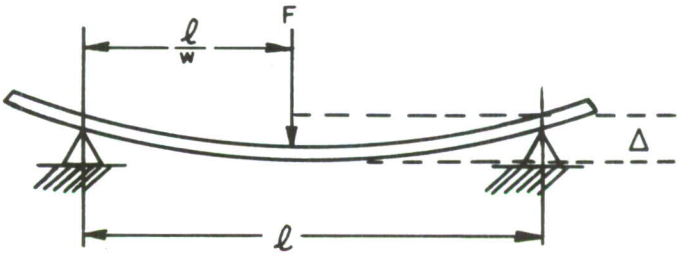

Applying center loading to the stripped board, the stiffness k and deflection Δ are recorded.

Thus: $E = \frac{\ell^3}{4bt^3} \cdot \frac{F}{\Delta}$ Where: $\frac{F}{\Delta} = k$

For board A

$$E = \frac{(7.9)^3\ (10)\ (13.1)}{4\ (6)} = 1.14 \times 10^6\ \#/in.^2$$

The modal density is,

$$n(f) = \frac{A_p \sqrt{3}}{C_L t}$$

and $$C_L = \sqrt{\frac{E}{p}} = \sqrt{\frac{1.14 \times 10^6}{1.95\quad 10^{-4}}} = 77.5 \times 10^3\ in./sec$$

thus,

$$n(f) = \frac{51\ (1.73)}{77.5\ (10^3)\ (.0625)} = .0182\ modes/CPS$$

or,

n(f) = 18.2 modes/1000 CPS

For board B

$$E = \frac{(7.1)^3\ (16)^3\ (29.5)}{4\ (7)} = 1.5 \times 10^6\ \#/in.^2$$

and

$$C_L = \frac{1.5 \times 10^6}{2.22 \times 10^{-4}} = 82 \times 10^3\ in./sec$$

n(f) = no. of modes/CPS

k = 13.1 #/in.

l = 7.9 in.

b = width = 6 in.

t = thickness = 1/16 in.

w = weight of board = 0.24 #

$$p = \frac{w}{\text{volume} \times 386\ in./sec^2} = \frac{0.24}{8.5(6)\ (.0625)\ (386)} = 1.95 \times 10^{-4}\ \#\text{-sec}^2/in.^4$$

A_p = board area = 51 $in.^2$

C_L = longitudinal wave velocity (in./sec)

k = 24.5 #/in.

l = 7.1 in.

A_p = 59.5 $in.^2$

The model density is,

$$n(f) = \frac{59.5\ (1.73)}{82\ (10^2)\ (.0625)} = .020 \text{ modes/CPS}$$

$b = 7$ in.

$t = 1/16$ in. $= .0625$ in.

$W = .32\ \#$

$$p = \frac{.32}{3.72\ (.386)}$$

$$= 2.22 \times 10^{-4}\ \#\text{-sec}^2/\text{in.}^4$$

or

$$n(f) = 20 \text{ modes/1000 CPS}$$

Summarizing:

The mode density for board A is:

$$n\ (f) = 18.2 \text{ modes/1000 CPS}$$

The mode density for board B is:

$$n\ (f) = 20 \text{ modes/1000 CPS}$$

APPENDIX II

MODAL DENSITY CORRECTIONS FOR INCREASED MASS AND STIFFNESS OF COMPLETE BOARDS MOUNTED IN SITU

The board is mounted in the test jig and the stiffness k is determined as in Appendix I.

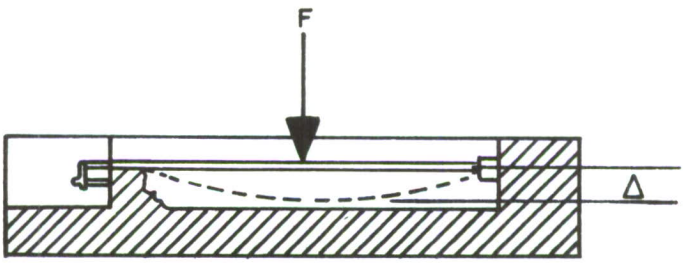

Dividing:

$$\frac{C_L}{C_L'} = \sqrt{\frac{E/\rho}{E'/\rho'}} \quad \text{setting:} \quad \frac{E'}{E} \propto \frac{k'}{k}$$

$$\frac{p}{p'} \propto \frac{w}{w'}$$

Thus:

$$C_L' = C_L \sqrt{\frac{k'}{k} \cdot \frac{w}{w'}}$$

Solving for C_L for board A

Where:

k = stiffness of board A (stripped) (13.1 #/in)

k' = stiffness of complete circuit board mounted in jig (76 #/in)

w = weight of board stripped of stiffners and components (0.24#)

w' = weight of board with components and stiffeners (.62#)

C_L = longitudinal wave velocity of stripped board (77.5×10^3 in/sec)

C_L' = pseudo, or adjusted C_L

E and E' = Youngs Modulus for stripped and original boards, respectively

ρ and ρ' = density of stripped and original boards, respectively

n(f) = mode density of stripped board

n(f)' = mode density of complete (and mounted) board

For Board A

$$C_L' = 77.5 \times 10^2 \sqrt{\frac{76}{13.1} \cdot \frac{0.24}{0.62}} = 72.2 \times 10^3 \sqrt{2.25}$$

$$C_L' = 77.5 \times 10^3 \quad (1.5) = 116 \times 10^3 \text{ in./sec}$$

Dividing:

$$n(f) = \frac{A_p \sqrt{3}}{t\, C_L} \text{ by } n(f)' = \frac{A_p \sqrt{3}}{t\, C_L'}$$

We obtain:

$$\frac{n(f)}{n(f)'} = \frac{C_L'}{C_L}$$

$$n(f)' = \frac{C_L'}{C_L} n(f) \tag{18}$$

$$n(f)' = \frac{77.5}{116} \quad (18.2) = 12.1 \text{ modes/1000 CPS}$$

For Board B

$$C_L' = 104 \times 10^3 \sqrt{\frac{k'}{k} \cdot \frac{w}{w'}}$$

$$C_L' = 104 \times 10^3 \sqrt{\frac{116}{24.5} \quad \frac{0.32}{1.19}} = 104 \times 10^3 \sqrt{1.27}$$

$$C_L' = 104 \times 10^3 \quad (1.13) = 118 \times 10^3 \text{ in./sec}$$

Where:

$k = 24.5$ #/in.

$w = 0.32$ #

$k' = 116$ #/in.

$w' = 1.13$ #

$C_L = 104 \times 10^3$ in/sec

Substituting in Equation 18

$$n(f) = \frac{104}{118} \quad (20) = 17.7 \text{ modes/1000 CPS}$$

Summarizing:

For board A, $n(f)' = 12.1$ modes/1000 CPS

For board B, $n(f)' = 17.7$ modes/1000 CPS

APPENDIX III

DETERMINATION OF FREQUENCIES BELOW WHICH A GIVEN NUMBER OF MODES ARE CONTAINED

For a simply supported plate we have:

$$N(\omega_{mn} < \omega) = \frac{1}{4\pi}\left[\frac{A_p\,(\omega)^2}{(c)^2} - P\,\frac{(\omega)}{(c)} + \pi\right]$$

Where:

N = number of modes

ω = frequency (rads/sec)

A = area of plate (in^2)

P = perimeter of plate (in)

c = $\sqrt{\omega KC}$ = wave velocity (in/sec)

K = radius of gyration of plate section = $\frac{t}{V12}$

t = plate thickness

C_L = longitudinal wave velocity

We set N = 3, and rearranging the above equation, we have:

$$A\,\frac{(\omega)^2}{(c)^2} - P\,\frac{(\omega)}{(c)} - 11\pi = 0\text{, which has the quadratic form:}$$

$$Ax^2 + B_x + C = 0$$

Where:

$$A = A$$

$$B = -P$$

$$C = -11\pi$$

$$x^2 = \frac{\omega^2}{c^2}\text{, where } c = \sqrt{\omega KC_L}$$

Thus

$$f = \frac{KC_L x^2}{2\pi}$$

Solving for the root

$$x = \frac{(-B) \pm \sqrt{B^2 - 4AC}}{2A}$$

$$= \frac{P \pm \sqrt{(P)^2 - (44\pi)(51)}}{2A}$$

$$= \frac{29 \pm \sqrt{841 + 7050}}{102}$$

$$= \frac{29 \pm 7891}{102} = \frac{29 \pm 88.8}{102} = 1.05$$

$$f = \frac{KC_L' (x^2)}{2\pi} = 333 \ (x^2) = 333 \ (1.05)^2$$

$$f = 367 \text{ CPS}$$

Where:

$$P = 29 \text{ in.}$$

$$A = 51 \text{ in.}^2$$

$$C = -11\pi$$

$$4AC = -7050 \text{ in.}^2$$

$$K = \frac{t}{\sqrt{12}} = \frac{1}{16\sqrt{12}}$$

$$C_L' = 116 \times 10^3 \text{ in./sec}$$

For the case N = 1, the modal equation is:

$$A \frac{(\omega)^2}{(c)^2} - P \frac{(\omega)}{(c)} - 3\pi = 0$$

Proceeding as before, f = 214 CPS.

UNCLASSIFIED

Security Classification

DOCUMENT CONTROL DATA - R & D

(Security classification of title, body of abstract and indexing annotation must be entered when the overall report is classified)

1. ORIGINATING ACTIVITY *(Corporate author)*	2a. REPORT SECURITY CLASSIFICATION
Air Force Flight Dynamics Laboratory Air Force Systems Command Wright-Patterson Air Force Base, Ohio 45433	UNCLASSIFIED
	2b. GROUP

3. REPORT TITLE

THE PREDICTION OF INTERNAL VIBRATION LEVELS OF FLIGHT VEHICLE EQUIPMENTS USING STATISTICAL ENERGY METHODS

4. DESCRIPTIVE NOTES *(Type of report and inclusive dates)*

Technical Report — June 1965 to October 1967

5. AUTHOR(S) *(First name, middle initial, last name)*

Robert W. Sevy
David L. Earls

6. REPORT DATE	7a. TOTAL NO. OF PAGES	7b. NO. OF REFS
January 1970	71	6

8a. CONTRACT OR GRANT NO.	9a. ORIGINATOR'S REPORT NUMBER(S)
b. PROJECT NO. 1309	AFFDL-TR-69-54
c. Task No. 130904	9b. OTHER REPORT NO(S) *(Any other numbers that may be assigned this report)*
d.	

10. DISTRIBUTION STATEMENT This document is subject to special export controls and each transmittal to foreign governments or foreign nationals may be made only with prior approval of the Air Force Flight Dynamics Laboratory (FDFE), Wright-Patterson Air Force Base, Ohio 45433

11. SUPPLEMENTARY NOTES	12. SPONSORING MILITARY ACTIVITY
	Air Force Flight Dynamics Laboratory (FDFE) Air Force Systems Command Wright-Patterson Air Force Base, Ohio 45433

13. ABSTRACT

This study is primarily concerned with the prediction of internal vibration levels in an equipment package using statistical energy methods. Modal densities, loss and coupling factors were determined theoretically and experimentally. Predicted vibration levels were derived and compared to experimental results. The energy coupling factor relating the box cover to the internal component responses was derived and compared favorably to experimental values. A generalized coupling factor is included for future applications. It is demonstrated that statistical energy methods offer a new and powerful method by which the average internal vibration levels of equipments may be predicted when the vibration field of the equipment cover is known or can be estimated.

This abstract is subject to special export controls and each transmittal to foreign governments or foreign nationals may be made only with prior approval of the Air Force Flight Dynamics Laboratory (FDFE), Wright-Patterson Air Force Base, Ohio 45433.

DD FORM 1 NOV 65 1473

UNCLASSIFIED

Security Classification

14. KEY WORDS	LINK A		LINK B		LINK C	
	ROLE	WT	ROLE	WT	ROLE	WT
Prediction						
Vibration						
Equipment						
Statistical Energy						
Coupling						
Loss Factor						